An adaptive local maximum entropy point collocation method for linear elasticity

Lei Fan[1*], William M. Coombs[2], Charles E. Augarde[2]

[1] *Department of Mechanical Engineering, Michigan State University, US*
[2] *Department of Engineering, Durham University, UK*

Abstract

Point collocation methods are strong form approaches that can be applied to continuum mechanics problems and possess attractive features over weak form-based methods due to the absence of a mesh. While various adaptive strategies have been proposed to improve the accuracy of weak form-based methods, such techniques have received little attention for strong form-based methods. In this paper, combined rh-adaptivity, in which r- and h-adaptivities are adopted iteratively, is applied to the local maximum entropy point collocation method for the first time to solve linear elasticity problems. Material force residuals act as driving forces in r-adaptivity to relocate collocation points, reducing the error associated with a given point distribution. Physical equilibrium residuals are used as the error estimator in h-adaptivity to determine the insertion locations for new points, diminishing the error caused by inadequate degrees of freedom. Issues arising in mesh-based methods, such as mesh distortion and hanging nodes, are entirely absent from the proposed method. The paper introduces the approach for the first time and the study is therefore confined to 2D domains. Numerical examples are presented to demonstrate the performance of the proposed adaptive strategies, comparing convergence rates and computational costs using uniform refinement, pure r-, h- and combined rh-adaptivities.

Keywords: Point collocation, rh-adaptivity, error estimation

1. Introduction

In the approximate solution of continuum mechanics problems, mesh-based methods experience challenges when dealing with features such as large deformation and discontinuities because of the use of a mesh. For this reason, meshless methods, in which the problem domain and boundaries are discretised by points or nodes, continue to be of interest to researchers. Meshless methods are generally divided into either weak or strong form-based methods [1, 2]. In the latter category, the most widely known are the point collocation methods (PCMs) [3–5] which work with a discretised strong form where the governing partial differential equations (PDEs) and boundary conditions of the problem are enforced

*Corresponding author. Tel.:+01 8598030086.
Email address: leifan0522@gmail.com (Lei Fan[1])

at a set of discrete collocation points rather than in a volume averaged sense over the domain as in a weak form approach [6]. The resulting linear system of equations in terms of displacement are solved at discrete source points, data which can then be used to approximate the solution at any point in the problem domain. Compared to weak form-based meshless methods, collocation methods remove the need for integration, and an associated mesh of integration cells, making implementation simple and straightforward [7]. However, greater complexity arises in strong form methods in the approximation of higher order derivatives than in the weak form case, which can lead to time-consuming calculation of basis functions and their associated derivatives.

The linear system for a PCM is built by writing the PDE or a displacement boundary condition at a given collocation point in terms of products of unknown displacements at, and basis functions associated with, the source points. Various basis functions have been proposed for PCMs in the literature, such as reproducing kernel basis functions [8, 9], radial basis functions [10–12] and discrete least squares basis functions [13, 14] but most do not possess the Kronecker-delta property, making the direct imposition of displacement boundary conditions inaccurate. These difficulties also affect weak form-based methods where there has been considerable investigation of this problem (for a review see [15]), and a number of techniques have been proposed to deal with this problem including a combination of the element-free Galerkin method (EFGM) with finite element method (FEM) basis functions near boundaries [16] and the adoption of Lagrange multipliers [1]. Although these methods can be used approximately to impose displacement boundary conditions, they have some disadvantages. The combination of the EFGM with FEM basis functions near boundaries, possesses the Kronecker-delta property on boundaries but the construction of FEM basis functions requires meshes and the interface of the coupled methods needs to be addressed properly [16]. Lagrange multipliers can impose displacement boundary conditions accurately, however, additional unknowns are introduced in addition to the original field variables, resulting in an increased problem size and in some cases, changing the nature of the coefficient matrix in the linear system to be solved [1].

One solution to the drawbacks mentioned above is to adopt local maximum entropy (max-ent) basis functions [17], which were originally derived from ideas in information theory and the max-ent principle [18, 19]. The local max-ent basis functions with the linear consistency have been applied to solve linear and nonlinear problems [20], and fourth order PDEs [21]. Crack propagation in Kirchhoff-Love thin shells with complex surface geometries has been modelled by the local max-ent approximants with linear reproducing conditions [22]. Local max-ent basis functions, together with enrichment functions used in partition of unity methods have also been employed to discretize problems in linear elastic fracture mechanics, improving accuracy relative to the standard extended finite element method at a comparable computational cost [23]. First order max-ent basis functions, have also been extended to the second order basis functions [24] for solving problems such as structural vibrations [25] and incompressible media problems [26]. A local max-ent basis function based point collocation method (MEPCM) was

recently proposed by the authors in [27]. The method possesses a number of advantages over existing strong form-based methods. The satisfaction of the weak Kronecker-delta property on boundaries eliminates the error at those collocation points, improving the overall accuracy. Some variables used in implementing the max-ent basis functions can be reused in calculating the basis function derivatives, which reduces the computational cost. The MEPCM is used for the research presented in this paper. Recently, the same idea was extended, in [28] who presented a point collocation method based on higher-order local max-ent basis functions than used in the original MEPCM.

Discretisation errors in a numerical solution that are caused by the imbalance of the governing equations and boundary conditions at individual points (or nodes), can be split into sources arising from improper distribution of points, an inadequate number of degrees of freedom and inadequacy of the solution space [29, 30]. Uniform h-refinement in which new points are added so that the distances between any two nearest points are reduced uniformly is the easiest way to reduce the error but is inefficient because increased computational cost arises due to new points being introduced to regions with very low errors. An alternative is to follow an adaptive process comprising of an error assessment which then informs a refinement strategy, aiming to balance accuracy with computational cost. There are three types of adaptive strategies: r-, h- and p- adaptivities, depending on the error measure (error measure in r-adaptivity needs to provide a direction of movement) and refinement strategy chosen. The main idea of h-adaptivity is to increase the number of degrees of freedom by refining the mesh in mesh-based methods, or by inserting additional points in meshless methods locally to reduce the discretisation errors in the solution [31]. r-adaptivity means maintaining the same number of degrees of freedom and the order of the field variable approximation, but altering locations of points [32]. p-adaptivity works by changing the order of the basis functions [33].

The objective of this paper is to present the first adaptive versions of the MEPCM using three strategies: h-, r- and rh-. All are potentially attractive for the MEPCM and any PCM, where relocation of existing or addition of new collocation and source points can be implemented without being concerned with remeshing. r-adaptivity, in which points are relocated driven by material force residuals, is combined here with h-adaptivity in which the error is estimated by residuals of the physical equilibrium equations. In the combined case, r- and h-adaptivities are used alternately. While there are some properties of the basis functions that are the subject of ongoing research, as discussed below, the goal of the paper is to demonstrate the approach using numerical results.

2. Adaptivity

2.1. h-adaptivity

h-adaptivity approaches require error estimators to estimate the difference between exact and approximated solutions and to identify the errors for refinement. In elasticity problems, as the exact solution is unknown in most practical cases, a "recovered" stress, obtained by a recovery technique, is used to

replace the exact solution in error estimators. The superconvergent patch recovery technique proposed by Zienkiewicz and Zhu in [34] is one of the most popular recovery methods in the FEM, where the recovered stress values are interpolated based on nodal values and derivatives of basis functions [35]. Error estimators can be computed in an energy norm depending on the difference between the recovered and approximated stress fields. This can be done, for example, at a point or in an individual element in adaptive isogeometric analysis (IGA) [36] and adaptive IGA-collocation (IGA-C) approaches [37]. Since the superconvergent patch recovery technique is simple to implement, as explained in [38, 39], this measure has been widely used in mesh-based methods applied to hyperbolic problems [40] and 2D planar elasticity problems [41]. Taking this idea to meshless methods the "recovered" stress has been revised to a "projected" stress, which is computed in a different way [42] such as its use in the reproducing kernel particle method (RKPM) [43, 44]. The projected stress values are evaluated using the same discretisation as the approximation but with reduced influence domains at points [45]. Error estimation for strong form-based meshless methods has been investigated although the available literature is very limited. Errors have been estimated using the residuals of the governing equations at a set of individual points directly in [46, 47] who report that this error estimate is simple and straightforward to implement.

Using h-refinement with meshless methods means inserting new points in regions with relatively high local errors. However, in weak form-based meshless methods, adding new points usually comes with a computational overhead associated with revising the mesh for integration. When integration is performed over a background mesh, which does not coincide with the original basis function support, additional computational cost is required to remesh. One way to tackle this is to use nodal integration. However local refinement in weak form-based meshless methods makes the treatment of conforming nodal discretisation complicated because of the need for a Voronoi diagram. It is also time-comsuming for non-conforming methods as some constraints have to be satisfied to make integration accurate [48]. Refinement for strong form-based PCMs has been developed in [46, 47, 49, 50], where new collocation points are inserted to local regions with high local errors directly. In contrast to weak form-based meshless methods however, there is very little other literature on h-adaptive methods with PCMs to date.

2.2. r-adaptivity

In r-adaptivity, points are relocated rather than any new points being added. The distances and directions for point relocations are usually determined by error estimators based on the residual of the "material equilibrium" in terms of the Eshelby's material force, as derived in [51, 52]. The material force is used since it is concerned with the energetic changes of a continuum with respect to points' locations [53–55]. r-adaptivity has been applied mainly to FEM, as in [56–61], but the crucial issue arising in mesh-based r-adaptivity is element distortion. Errors can actually increase in r-adaptive FEM because of mesh distortion caused by the movement of nodes associated with an element [62–65]. To deal with

this, mesh optimisation has been used, e.g. in [66], where the movement of points is constrained to be sufficiently small by a step length parameter [67], however this can lead to an increased number of steps in optimization with extra computational cost.

Another drawback of r-adaptivity is that a specific accuracy may not be achievable with a given number of degrees of freedom. To tackle this, h-adaptivity can be used after a sequence of r-adaptive steps to further reduce discretisation errors. In [68], r- and h-adaptive strategies were used in two subdomains separately without refinement on the interfaces to exploit the advantageous properties of both strategies. Comparisons in terms of accuracy and convergence speed using pure and combined adaptive strategies were also conducted in [69, 70] where a combined rh-adaptive approach was shown to be more efficient than pure r- or h-adaptivity. Combined rh-adaptivity was also studied in [71, 72] for bimaterial interface problems, where discretisation errors were reduced in successive adaptive steps and the best sequence for combining the effectiveness of r- and h-adaptivity was studied. The efficiency of using combined rh-adaptivity was compared with pure h-adaptivity in [71] finding that a smaller number of degrees of freedom was required in the combined strategy than in pure h-adaptivity. In relation to the present study, to the best of the authors' knowledge, there is currently no literature on combined rh-adaptivity for PCMs and this gap provides an impetus for the research presented here. The key novelty of this work is to develop r-, h- and combined rh-adaptivities in the strong form-based MEPCM for the first time, improving the computational accuracy in terms of convergence rate as compared to uniform refinement. The proposed approach introduces some key advantages compared to weak form-based methods, which are discussed later.

3. Background to the MEPCM

The detailed formulation of the MEPCM is given in this section based on the approach [27].

3.1. Point collocation methods

Consider a boundary value problem in a 2D domain Ω governed by the PDE

$$\mathscr{L}\{u\} = \{f^b\} \text{ in } \Omega, \tag{1}$$

and boundary conditions

$$\mathscr{L}_u\{u\} = \{g\} \text{ on } \Gamma_u \text{ and } \mathscr{L}_t\{u\} = \{h\} \text{ on } \Gamma_t, \tag{2}$$

where $\{u\}$ is the vector of field variables, $\mathscr{L}$ is the differential operator in Ω, $\mathscr{L}_u$ and $\mathscr{L}_t$ are the differential operators for displacement (Dirichlet) and traction (Neumann) boundary conditions respectively, $\{f^b\}$ is the vector of body forces, $\{g\}$ and $\{h\}$ are the prescribed displacement and traction vectors on the displacement boundary, Γ_u, and the traction boundary, Γ_t respectively. In PCMs, the problem domain and boundaries are discretised by collocation and source points numbering N_c and N_s respectively. The governing PDEs and boundary conditions are applied to collocation points, formulating the

system of equations in terms of the field variable at source points. N_s^* source points having non-zero basis function values contribute to the approximation at a given collocation point, the collection of these source points often being referred to as the "support" of the collocation point. The vector of field variables at source points, which is obtained by solving the system of equations, can be used to approximate the solution at any point $\{u^h\}$. To derive the linear system using a PCM, one imposes the appropriate condition from Eq. (1) and (2) at each collocation point in the interior of the domain and at boundaries, leading to a discrete set of equations in terms of the field variable vector at source points, $\{d\}$, of the form

$$[K]\{d\} = \{f\}. \tag{3}$$

In Eq. (3), the entries of $[K]$ are the differential operators with basis functions or derivatives, so for 2D elasticity problems the size of the coefficient matrix $[K]$ is $2N_c \times 2N_s$. Note that $[K]$ is generally asymmetric. The sizes of the unknown $\{d\}$ and known right-hand side vector $\{f\}$ are $2N_s \times 1$ and $2N_c \times 1$, respectively. As an example, the differential operators for 2D plane strain elasticity problems are summarised in Table 1 where the scale D

$$D = \frac{E(1-\nu)}{(1+\nu)(1-2\nu)}. \tag{4}$$

The number of collocation points has to be equal to or exceed the number of source points. When $N_c = N_s$ a square system is formed and a unique solution can be obtained. However, when $N_c > N_s$ an overdetermined system is obtained and a suitable solver (e.g. the least squares method) must be employed [8]. In this paper, the same number of collocation and source points is generated for the initial discretisation in all the numerical examples. Once $\{d\}$ has been determined the approximation at any point can be evaluated by

$$\{u^h(x,y)\} = [\phi_s(x,y)]\{d_s\}, \tag{5}$$

where $\{u^h\}$ is the approximation of the solution at one point, $[\phi_s(x,y)]$ and $\{d_s\}$ represent a matrix of basis function values and a vector of field variables associated with the source points inside the support of the point.

Operator	2D Elasticity
$\mathscr{L}$	$D\begin{bmatrix} \frac{\partial^2}{\partial x^2} + \frac{1-2\nu}{2(1-\nu)}\frac{\partial^2}{\partial y^2} & \frac{1}{2(1-\nu)}\frac{\partial^2}{\partial x \partial y} \\ \frac{1}{2(1-\nu)}\frac{\partial^2}{\partial x \partial y} & \frac{\partial^2}{\partial y^2} + \frac{1-2\nu}{2(1-\nu)}\frac{\partial^2}{\partial x^2} \end{bmatrix}$
$\mathscr{L}_u$	$\begin{bmatrix} 1 & 0 \\ 0 & 1 \end{bmatrix}$
$\mathscr{L}_t$	$D\begin{bmatrix} \frac{\partial}{\partial x}n_x + \frac{1-2\nu}{2(1-\nu)}\frac{\partial}{\partial y}n_y & \frac{\nu}{1-\nu}\frac{\partial}{\partial y}n_x + \frac{1-2\nu}{2(1-\nu)}\frac{\partial}{\partial x}n_y \\ \frac{1-2\nu}{2(1-\nu)}\frac{\partial}{\partial y}n_x + \frac{\nu}{1-\nu}\frac{\partial}{\partial x}n_y & \frac{1-2\nu}{2(1-\nu)}\frac{\partial}{\partial x}n_x + \frac{\partial}{\partial y}n_y \end{bmatrix}$

Table 1: The differential operators for 2D elasticity problems.

3.2. Maximum entropy basis functions

The concept of max-ent comes from probability theory [18, 19] where a set of mutually independent events $\{A_1, A_2, ..., A_n\}$ with unknown probabilities $\{p_1, p_2, ..., p_n\}$ are considered. The least biased probability distribution can be obtained by maximising the informational entropy $P(\cdot)$ (the specific description of uncertainty) as

$$\text{maximise}\Big(P(p_1, p_2, ..., p_n) = -\sum_{a=1}^{n} p_a \log p_a\Big), \tag{6}$$

where p_a is the probability associated with the occurrence of the event A_i. If probabilities are replaced by basis functions in a defined domain, the partition of unity property is automatically satisfied. The linear reproducing conditions, which must also be satisfied, can be applied as constraints on the max-ent basis functions, written (in the 1D case) as

$$\sum_{s=1}^{N_s^*} \phi_s = 1 \quad \text{and} \quad \sum_{s=1}^{N_s^*} \phi_s x_s = x, \tag{7}$$

where s is the index of a source point inside the support of a collocation point. The local max-ent basis function can be formulated as

$$\phi_s(\{x\}) = \frac{Z_s}{Z}, \tag{8}$$

where

$$Z_s = w_s e^{-\{\bar{\lambda}_s\}^T(\{x_s\}-\{x\})}, \quad \text{and} \quad Z = \sum_{s=1}^{N_s^*} Z_s. \tag{9}$$

In Eq. (9), $\{\bar{\lambda}\}$ denotes the unique Lagrange multiplier that is determined via a Newton-Raphson method combined with $\{\bar{\lambda}\} = \text{arg min } \log Z(\{x\}, \{\bar{\lambda}\})$ [25] and w_s is the weight function that control the locality of basis functions. For the MEPCM used here, a cubic spline is used as the weight function, which is expressed in 1D as

$$w(x - x_s) = w(r) = \begin{cases} \frac{2}{3} - 4r^2 + 4r^3 & 0 < r \leq \frac{1}{2} \\ \frac{4}{3} - 4r + 4r^2 - \frac{4}{3}r^3 & \frac{1}{2} < r \leq 1 \\ 0 & r > 1 \end{cases}, \tag{10}$$

where

$$r(x - x_s) = \frac{\|x - x_s\|}{d_m} \tag{11}$$

is the normalised radius of the support domain, $||x - x_s||$ is the distance between the sth source point and collocation point of interest x and d_m is a user-defined parameter. In this paper we adopt

$$d_m = d_{max}\ dx, \tag{12}$$

where the scaling parameter d_{max} is typically $2.0 - 4.0$ and dx is the distance between the collocation point and the nearest source point in its support domain. The MEPCM used in this paper is for 2D problems and the basis functions are tensor products of the 1D max-ent basis functions described above,

and therefore have square support domains. This is significantly different from some other examples in the literature where 2D max-ent functions are produced using radial basis weight functions, e.g. [73, 74]. The two approaches have other differing properties that are discussed below.

Max-ent basis functions defined over a convex domain satisfy a weak Kronecker-delta property at the boundary while on non-convex domains this can be lost in some cases [17]. In practice, however, max-ent basis functions have been shown to perform well on non-convex domains for elasticity problems [20].

The max-ent basis functions described above have linear consistency which, if used with radial basis weight functions, can be shown to be safe to use, on convergence grounds, to solve problems with at most first-order derivative terms, such as encountered in weak form elasticity, for instance. Higher order max-ent basis functions have been developed and used successfully in [25, 28] for problems requiring higher order consistency. However, a number of studies have demonstrated numerical evidence of very good convergence using max-ent basis functions with linear consistency, with fourth order PDEs discretised with a weak form approach [21] and by the current authors for second order PDEs using the MEPCM [27], and indeed in the results later in this paper. The key aspect of the MEPCM used here that may explain this is the fact that a tensor product of two 1D basis functions is used to form the 2D basis, unlike the radial basis used in many other published cases, and research is underway to explore this behaviour to appear in a future paper.

4. Adaptive strategies for the MEPCM

In this section, r- and h-adaptive procedures are described for the 2D MEPCM, where collocation points are relocated and more collocation and source points are introduced locally, respectively.

4.1. r-adaptive strategy

We employ an r-adaptive approach using an error estimator based on residuals of material (rather than physical) equilibrium for small deformation problems in 2D linear elasticity. Material equilibrium is based on the Eshelby stress (or momentum tensor) [75, 76] rather than the Cauchy stress in physical equilibrium. Material equilibrium in the absence of body forces takes the following form

$$[L]^T\{\Sigma\} = \{0\} \quad \text{in } \Omega, \tag{13}$$

where $[L]$ is a matrix of differential operators

$$[L] = \begin{bmatrix} \frac{\partial}{\partial x} & 0 \\ 0 & \frac{\partial}{\partial y} \\ \frac{\partial}{\partial y} & \frac{\partial}{\partial x} \end{bmatrix}, \tag{14}$$

$\{\Sigma\}$ is the Eshelby stress, $\{0\} = \{0, 0\}^T$ and Ω is the problem domain. The residuals of the material equilibrium are adopted as the error estimator

$$[L]^T\{\Sigma\} = \Big\{\frac{\partial W}{\partial x}\Big\}_{\text{explicit}}, \tag{15}$$

where $\Big\{\frac{\partial W}{\partial x}\Big\}_{\text{explicit}}$ are the explicit derivatives of the strain energy with respect to $\{x\}$. Coordinates $\{x\}$ label each particle of the medium, which corresponds to the position it occupies in the problem domain. The derivation Eq. (15) can be found in Appendix A.

The non-optimal locations of collocation points act to disrupt the achievement of material equilibrium in a similar way to the disruption a defect in a material has in a mechanical problem as explained in Eshelby's original work [75] and the subsequent literature on configurational mechanics for fracture. The Cauchy stress describes the deformed state with respect to displacement while the Eshelby stress is related to the global energy change of the deformed solid with respect to the collocation point positions. The imbalance of the material equilibrium can therefore be seen as a result of an inefficient discretisation [71]. The residual in the divergence of the Eshelby tensor therefore becomes the error estimator and r-adaptivity is accomplished by minimising the residual in Eq. (15) with respect to collocation point locations. Using PCMs, the discrete strain energy can be calculated via

$$\begin{aligned} W &\cong \sum_{c=1}^{N_c} \frac{1}{2}\{\sigma\}_c^T\{\varepsilon\}_c V_c \\ &\cong \sum_{c=1}^{N_c} \frac{1}{2}\Big\{[L]\{u\}\Big\}_c^T [D^e]\Big\{[L]\{u\}\Big\}_c V_c, \end{aligned} \tag{16}$$

where $\{\sigma\}= \{\sigma_{xx}, \sigma_{yy}, \sigma_{xy}\}^T$ is the vector of the Cauchy stress, $\{\varepsilon\}= \{\varepsilon_{xx}, \varepsilon_{yy}, \gamma_{xy}\}^T$ is the vector of strain, V_c denotes a volume (i.e. an area in 2D and a length in 1D) associated with each collocation point and computed via a Voronoi diagram, $\{u\}$ is the displacement vector, $[D^e]$ is the elastic stiffness matrix given by

$$[D^e] = \frac{E}{(1+\nu)(1-2\nu)}\Big[(1-2\nu)[I] + \nu\{1\}\{1\}^T\Big], \quad \text{with} \quad \{1\} = \{1 \;\; 1 \;\; 0\}^T, \tag{17}$$

and $[I]$ is the identity matrix. The residual $\{R(x)\}$ of the material equilibrium given in Eq. (15) can be the explicit derivative of strain energy in Eq. (16) with respect to collocation point locations $\{x_c, y_c\}^T$, i.e.

$$\{R(x)\} = \Big\{\frac{\partial W}{\partial x_c}, \frac{\partial W}{\partial y_c}\Big\}^T, \tag{18}$$

where c represents the index of collocation points. The physical equilibrium for elasticity problems is linearly dependent on the displacement, however the material equilibrium is not, as non-linear terms of the displacement are included in Eq. (18). The Newton-Raphson method is used to solve the non-linear system of equations. The new positions of collocation points at an iterative step $n+1$ can be found by

$$\{x_{n+1}\} = \{x_n\} - [R'(x_n)]^{-1}\{R(x_n)\}, \tag{19}$$

where n is the nth Newton-Raphson iterative step, $\{x_n\}$ and $\{x_{n+1}\}$ are the estimate of positions in the previous step and the new positions in the current step. $[R'(x_n)]$ is the derivative of the residual vector $\{R(x_n)\}$ with respect to collocation point coordinates. The second term on the right-hand side of Eq. (19) indicates the moving direction and distance for a collocation point. Eq. (19) can be solved pointwise and the explicit form of $[R'(x)]$ is

$$[R'(x)]_c = \begin{bmatrix} \frac{\partial^2 W}{\partial x_c^2} & \frac{\partial^2 W}{\partial x_c \partial y_c} \\ \frac{\partial^2 W}{\partial x_c \partial y_c} & \frac{\partial^2 W}{\partial y_c^2} \end{bmatrix}. \tag{20}$$

In Eq. (20), the third derivatives of max-ent basis functions are required in the second derivatives of strain energy W with respect to the current position of each collocation point and are calculated using forward difference method based on the second derivatives of basis function values. The detailed formulations of the residual vector in Eq. (18) and its derivatives in Eq. (20) for 1D problems are given in Appendix B. Since collocation points are independent of each other, the mixed second derivatives of strain energy with respect to two different collocation points are zero. Once the residual in the Newton-Raphson method passes a defined convergence criterion the updated positions of the collocation points are obtained. As the values of residual norms vary with problems, it is difficult to define a specific tolerance in general. The relative residual norm η_r^n is used here defined as

$$\eta_r^n = \frac{||\Delta R(x_n)||}{||R(x_n) + \Delta R(x_n)||}. \tag{21}$$

In Eq. (21), $||\cdot||$ is the L_2 norm where

$$||R(x)|| = \sqrt{\sum_{c=1}^{N_c} \left(\frac{\partial W}{\partial x}\right)_c^2}, \tag{22}$$

and $||\Delta R(x_n)||$ is the norm of the total material force residual difference between the $(n+1)$th and nth iteration steps. A typical value of η is 10^{-2}. r-adaptivity continues until the relative residual η_r satisfies $\eta_r < \eta$. In mesh-based methods, the relative residual norm η_r decreases initially, however η_r tends to go up in latter iterations due to progressive mesh distortion [77], however in PCMs, the relative residual norm is not influenced by mesh distortion.

In the implementation of r-adaptivity with the MEPCM, the displacement vector $\{d\}$ is used to calculate the material force residual vector $\{R\}$ and the tangent matrix $[R']$ in each Newton-Raphson iteration step. The positions of collocation points in the current iterative step can be determined by Eq. (19) directly. Additional constraints are employed so that collocation points on the boundaries are fixed normal to the boundaries. The vector $\{d\}$ is then recalculated using the collocation points obtained in each iterative step, and max-ent basis functions. As source points are not moved in r-adaptivity, max-ent basis functions are constructed based at the initially distributed source points in the overall r-adaptivity analyses. The reuse of basis functions can avoid to induce extra computational cost associated with recalculating basis functions.

4.2. h-adaptive strategy

In the proposed h-adaptivity strategy, local errors are estimated by the residuals of the physical equilibrium at some generated calculation points in local areas and these are then used to estimate error distribution in the overall domain, while their summation is adopted to estimate the global accuracy of the solution. In order to estimate errors over local areas, a Delaunay triangulation associated with

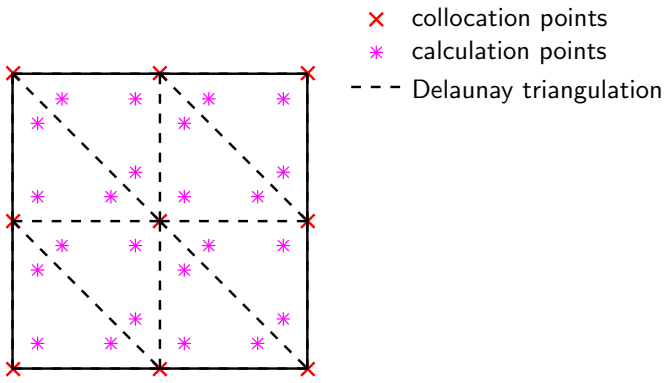

Figure 1: The generation of the Delaunay triangulation and calculation points in h-adaptivity (n_c=3 is selected here as a representation).

collocation points is generated (see Figure 1). The so-called calculation points in the proposed scheme are located at the Gauss quadrature points in these triangles. Arbitrary number of calculation points can be generated in each triangulation as these points are used for error estimation rather than numerical integration. For h-adaptivity the local error estimator is given as

$$e_t = \frac{1}{n_c} A_t \sum_{g=1}^{n_c} ||\mathscr{L}\{u^h(\{x_g\})\} - \{f^b(\{x_g\})\}||, \tag{23}$$

where n_c is the number of calculation points, $\frac{1}{n_c}A_t$ is the product of the Gauss point weight and the determinant of the Jacobian for the triangle under consideration, g is the index associated with the calculation point, A_t is the area of the tth Delaunay triangle, $\{x_g\}$ is the coordinates of the gth calculation point, $\{u^h\}$ is the approximation of solution. For elasticity problems, the residual of the strong form governing equations in Eq. (23) is replaced by the physical equilibrium equation. The global error estimator can then be easily obtained as

$$e_G = \frac{1}{A} \sum_{t=1}^{n_t} e_t, \tag{24}$$

where $A = \sum_{t=1}^{n_t} A_t$ is the total area of the Delaunay triangulation and n_t is the number of Delaunay triangles. The local and the global error estimators, e_t and e_G, developed for the MEPCM are used in the refinement procedure as described below.

The h-adaptive refinement strategy used here is based on mesh refinement ideas in weak form-based methods [78, 79] but is easier to implement without the constraints of point connectivity. The target is to reduce both local and global errors, achieving a prescribed accuracy. Here, a local refinement coefficient $k \in [0, 1]$ (uniform refinement with $k = 0$) is predefined. The permissible local error η_t is defined as

$$\eta_t = ke_{max}, \tag{25}$$

where e_{max} is the maximum local error. The selection of k is problem dependent and there is not a rule for the choice of the value of k. However, the choice of k is determined by the variation of local error estimators. A larger value of k could be chosen if local errors vary in a wide range while a smaller k is used if all local errors are close to each other. Triangles with $e_t > \eta_t$ are flagged for refinement and in which three new collocation and source points are inserted. Consider a discretisation with four

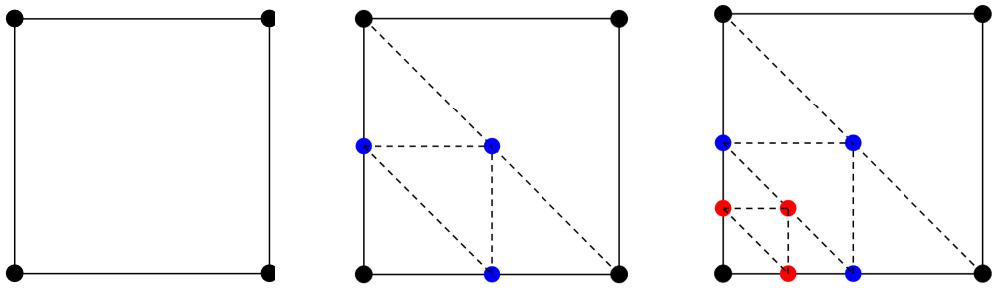

(a) Initial points distribution; (b) First refinement; (c) Second refinement.

Figure 2: Step by step points refinement in h-adaptivity.

points distributed as shown in Figure 2(a) in which two Delaunay triangles are generated. The lower triangle is flagged for refinement so three new points are added midsides of the triangle to create three new triangles for the next iteration as shown in Figure 2(b). A second refinement would occur as shown in Figure 2(c). For an irregular problem domain or randomly distributed points, refinement is still straightforward. In each h-adaptive step, some new points may be coincident with existing points, and have to be omitted. The new source points are situated at the same positions as the new collocation points and max-ent basis functions are recalculated when new source points are introduced. While a refined source point distribution improves the performance of max-ent basis functions, increased numbers of collocation points serve to better satisfy the governing PDEs and boundary conditions. h-adaptivity continues until the global error in Eq. (24) meets a prescribed value.

The effectiveness of the h-adaptive procedure can be described by an effectivity index as

$$\theta = \frac{e_G}{||e||_{L_2}}, \tag{26}$$

where e_G is the global error estimator and $||e||_{L_2}$ is the L_2 norm of relative error as

$$||e||_{L_2} = \frac{\sqrt{\{u^h - u^e\}^T\{u^h - u^e\}}}{\sqrt{\{u^e\}^T\{u^e\}}}. \tag{27}$$

In Eq. (27), $\{u^h\}$ and $\{u^e\}$ are the approximation and exact solution, respectively. The effectivity index can be measured for those problems with analytical solutions to validate the performance of the proposed error estimator. If the effectivity index, θ oscillates around a constant with an increasing number of degrees of freedom, the error estimate is efficient because the estimated error converges at a similar rate to the actual error.

r- and h-adaptivity can be employed in the MEPCM separately to improve accuracy, however both have their limitations. N_c and N_s are not changed in r-adaptivity; only the density of collocation points in the domain and on the boundaries is changed so in pure r-adaptivity, an arbitrarily prescribed accuracy may not be achievable using a given number of degrees of freedom. In pure h-adaptivity, although the number of points increases continuously, the positions of newly inserted points are at least partially determined by the initial distribution of points which presents a degree of inflexibility. Therefore, there is a potential advantage in combining the two approaches and a combined rh-strategy is also considered here, in which intermittent r- and h-adaptive steps occur. An arbitrarily defined accuracy η_g can be accomplished by an optimised point distribution with an optimal number of N_c and N_s. After the initial calculation using a given discretisation, r-adaptivity is used to adjust the point positions, which is followed by further h-adaptivity. As different quantities of error estimators are used in r- and h-adaptivity respectively, it is vital to point out that the given accuracy should be achieved by the residual η_r in r-adaptivity or e_G in h-adaptivity. In contrast to weak form-based methods, the need of integration, and an associated mesh can be removed in strong form-based MEPCM, making the implementation of the proposed rh-adaptivity in the MEPCM straightforward and efficient without mesh distortion in r-adaptivity and remeshing in h-adaptivity.

5. Implementation issues

While truly meshless methods do not possess connectivity information supplied by the presence of a mesh, basis functions and support domains around collocation points are needed. Sufficient source points are needed in the local support of each collocation point to guarantee the partition of unity (PoU) property.

In previous studies using max-ent basis functions, e.g. [20, 80], the size of the support domain for each collocation point was controlled by a scaling parameter d_{max}, making the choice of d_{max} vital as this support region has an influence on accuracy and stability of the approximation. For a regular distribution of source and collocation points, N_s^* is the same using a fixed d_{max} for most collocation points in the interior of the problem domain and the computational cost for calculating basis functions for each collocation point in the interior of the problem domain is similar. However, using a fixed d_{max}

in a random (or unstructured) distribution of points, as might occur with adaptivity, may lead to lengthy computational time for constructing basis functions for each collocation point as each will be different since N_s^* varies, but more seriously the coefficient matrix $[K]$ may be singular since there might be an insufficient number of points in support for some collocation points. In addition to this, for some collocation points on boundaries, fewer source points are likely to be included in the local support. An inapproaciate choice of d_{max} may cause ill-conditioning with high condition number or instabilities. To address this issue, an algorithm is used to search for the N_s^* nearest source points in the neighbourhood of each collocation point. The main idea is not to define a constant d_{max} but to define a minimum number of source points N_s^* in the support domain throughout the problem. These N_s^* nearest source points for each collocation point are stored for calculating basis functions. The minimum N_s^* could be set as three in 2D for linear basis functions, for example. An additional check is required to ensure that the N_s^* source points are not collinear with the collocation point in 2D (similar to the issue in [81] for weak form-based meshless methods). Using this idea, the computational cost for calculating basis functions of each collocation point is similar and singular coefficient matrices $[K]$ can be avoided. If the N_s^*th and (N_s^*+1)th source points have the same distances from the centred collocation point, both are included. A rectangular support domain is chosen as max-ent basis functions are constructed

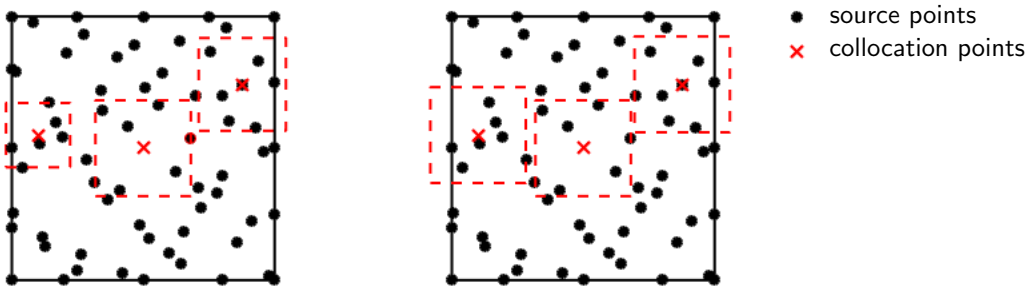

(a) Fixed N_s^* (b) Fixed size for support

Figure 3: Two algorithms for determining N_s^*.

in the Cartesian coordinates and the two different approaches used are as shown in Figure 3. In Figure 3(a) N_s^* is set as 6 for all collocation points and it can be seen that the sizes of support domain for all collocation points are different. Since coincident source and collocation points may lead to inaccuracy of the first max-ent basis function derivatives [82], source points that are identified in a search that are coincident with the collocation point are not counted in N_s^*. Figure 3(b) shows the case where the size and shape of support domain (i.e. d_{max}) is the same for all collocation points and N_s^* varies across the support domains. In the numerical examples section which follows, the performance in terms of accuracy using both methods, i.e. fixed N_s^* and fixed d_{max}, is demonstrated.

6. Numerical examples

In this section, some numerical examples are presented to demonstrate the performance of the proposed r-, h- and rh-adaptivity procedures. Comparisons in terms of accuracy using fixed N_s^* and d_{max} are conducted for r- and h-adaptivity separately. The first two examples have analytical solutions so that clear L_2 norms of relative errors $||e||_{L_2}$ can be determined to show convergence rates. The effectivenesses of the proposed error estimator in h-adaptivity is validated by comparing the plots of $||e||_{L_2}$ and e_G versus degrees of freedom. In h-adaptivity, two calculation points (n_c=2) are selected in each local length for 1D problems and three calculation points (n_c=3) are selected in each triangulation for 2D problems in order to keep the balance of accuracy and computational cost. All analyses were run in MATLAB R2015b using an Intel(R) Core(TM) i7-4790 CPU @ 3.60 GHZ. The computational efficiency with respect to accuracy and computational times are presented for each adaptivity strategy. The CPU times stated in the later examples are the averages from 10 measurements.

6.1. 1D bar

In this example, a 1D linear elastic bar of unit length fixed at the point $x = 0$ and subjected to a body force $f^b(x) = x$ is studied using r- and h-adaptivities respectively to validate each proposed individual adaptive approach. For this 1D problem, the linear system was set up with displacement boundary conditions imposed at collocation points at the two ends and the governing equation applied to all collocation points inside the domain. For small deformations, the analytical solutions for displacement and Cauchy stress are

$$u(x) = \frac{1}{E}\Big(\frac{x}{2} - \frac{x^3}{6}\Big) \quad \text{and} \quad \sigma(x) = \Big(\frac{1-x^2}{2}\Big), \tag{28}$$

where here, $E = 1.0$. The unit length bar was discretised by a uniform distribution of collocation points and source points at the same positions since the first max-ent basis function derivatives are not required in implementing boundary conditions here.

6.1.1. r-adaptivity

Eleven collocation and source points were distributed uniformly in the problem domain and at the boundaries. All source points were fixed during r-adaptivity. The residual norm $||R(x)||$ in Eq. (22) for each Newton-Raphson iterative step is presented in Figure 4(a) where $||R(x)||$ decreases rapidly in the first three steps followed by a degradation in the last two steps, converging to a non-zero value. It demonstrates that the discretisation errors cannot be further reduced with this given number of degrees of freedom, which is a limitation of pure r-adaptivity as stated above. The convergence of the Newton-Raphson method for this 1D bar problem is shown in Figure 4(b) where the gradients between pairs of steps are shown. The convergence rate in the first three steps is close to the theoretical value 2.0 [83] but becomes to 0.08 in the latter steps, which is limited by the number of points.

The comparison between analytical and numerical results in terms of displacement and stress against collocation points distribution ($N_c = 11$) in r-adaptivity is given in Figure 5 where they match well

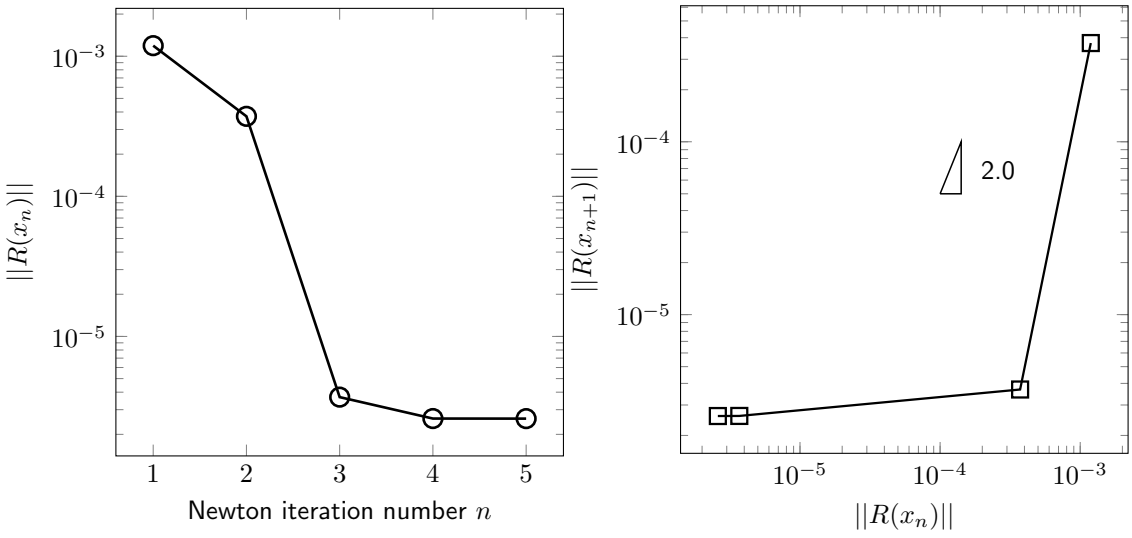

(a) $||R(x)||$ versus Newton iteration number.

(b) Convergence rate of $||R(x)||$.

Figure 4: Residual norms and convergence rate in the Newton-Raphson method of the 1D bar problem.

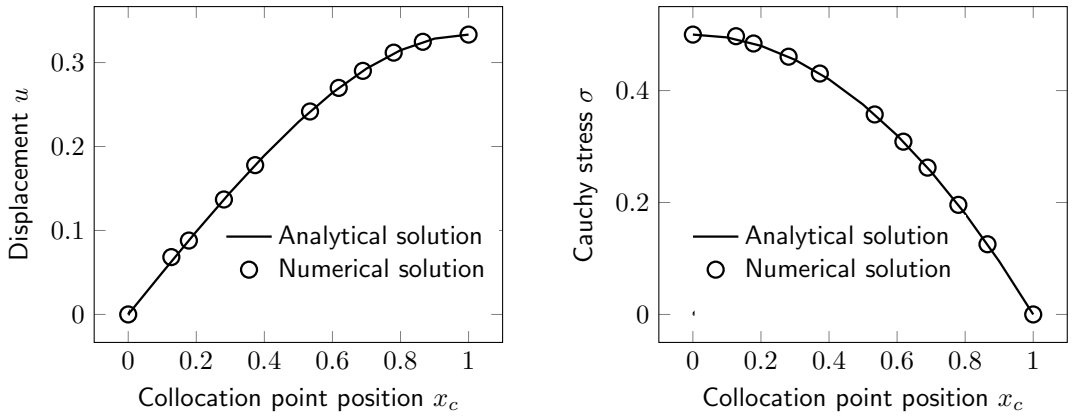

(a) Displacement results against positions.

(b) Stress results against positions.

Figure 5: Comparison in terms of displacement and stress between analytical and numerical results using the MEPCM for the 1D bar problem.

with each other. In Figure 6(a), a comparison in terms of the relative error $||e||_{L_2}$ given in Eq.(27) in uniform h-refinement and r-adaptivity with either fixed N_s^* or d_{max} is presented to show the influence of the choice for support domain. In this study, using $N_s^* = 2$ appears to achieve better convergence rates than using $N_s^* = 3, 4$ and $d_{max} = 2.0$. In Figure 6(a), the number of source points inside the local support N_s^* is critical to accuracy but it remains unclear how to find the optimal N_s^* theoretically [84]. Using fixed N_s^* makes the number of source points in the support the same for all collocation points but $N_s^* = 2, 3$ or 4 can result in different weight function values. When $N_s^* = 2, 3$ or 4, the condition number of the resultant coefficient matrix is smaller than 1000 without any ill-conditioning issues. Alternatively, using fixed d_{max} controls the size of support domain the same for each collocation point but N_s^* varies. Since in r-adaptivity, collocation points are gradually relocated to an irregular

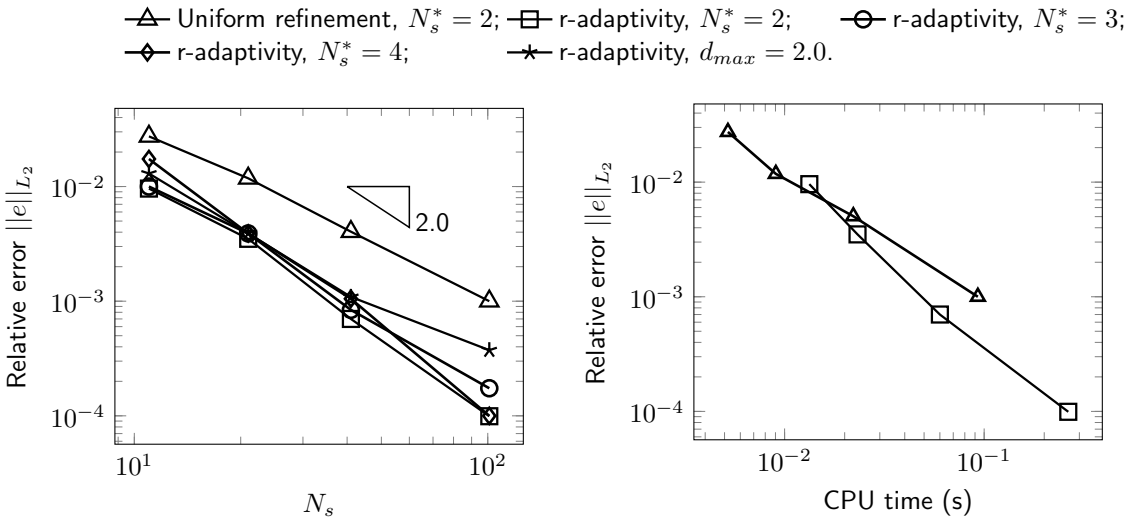

(a) Convergence rate of $||e||_{L_2}$; (b) Convergence rate of $||e||_{L_2}$ against CPU time.

Figure 6: Convergence rate of $||e||_{L_2}$ and computational efficiency of the 1D bar problem using uniform refinement and r-adaptivity with various N_s^*.

distribution, which may lead to deficiency in the linear system using $d_{max} = 2.0$. In Figure 6(b) CPU times for uniform h-refinement and r-adaptivity with $N_s^* = 2$ using different discretisations were measured to compare the computational efficiency. With the same number of degrees of freedom, uniform h-refinement is cheaper than r-adaptivity as r-adaptivity takes more time to find optimal positions for collocation points. However with an increasing number of degrees of freedom (relatively small errors), r-adaptivity with the MEPCM is more cost-effective than using uniform h-refinement because in uniform h-refinement the extra degrees of freedom are introduced in local regions with small errors. In this example, it is concluded that the accuracy of the MEPCM approximation can be improved through effective r-adaptivity.

6.1.2. h-adaptivity

The 1D bar is now analysed using h-adaptivity where the governing PDEs and boundary conditions are identical to those used in the study of r-adaptivity above. The initial discretisation is shown in Figure 7(a). In 1D analysis, the local error estimate e_t is replaced by e_l as

$$e_l = \frac{1}{2} l \sum_{g=1}^{2} ||E \frac{d^2 u_g^h}{dx_g^2} - x_g||, \tag{29}$$

which is estimated at the calculation points as shown in Figure 7(b) in each local length. In Eq. (29), l is the length between two adjacent collocation points, x_g is the coordinate of the gth calculation point and u_g^h is the approximation at the gth calculation point. The global error is

$$e_G = \frac{1}{L} \sum_{l=1}^{n_l} e_l, \tag{30}$$

where L is the length of the 1D problem domain and n_l is the number of individual lengths. In this example, new collocation and source points are added at the centres of local lengths determined by the local error estimate e_l.

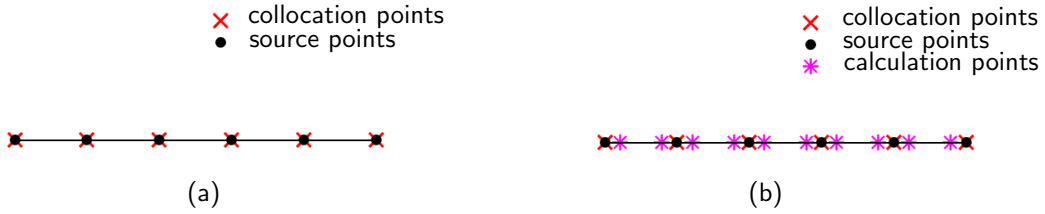

Figure 7: The collocation, source and calculation points generation in h-adaptivity of the 1D bar problem.

As shown in Figure 8, this study concerns the effect of the local refinement coefficient k ($k = 0.9, 0.95, 0.99$) on accuracy (both e_G and $||e||_{L_2}$) in h-adaptivity with $N_s^* = 2$. Although there is no theoretical value for the local refinement coefficient, k, the choice of k is affected by the variation of local errors over the domain. The range of local error in this example is small so k is selected to be close to 1. The global error estimator e_G given in Eq. (30) for uniform and h-adaptivity with $k = 0.9, 0.95, 0.99$ are plotted against N_s in Figure 8(a). It can be seen that e_G for uniform refinement decreases slower than h-adaptivity with $k = 0.9, 0.95, 0.99$. Using $k = 0.9$ allows more points to be added than using $k = 0.95$ and 0.99 in the adaptive steps. The convergence rate of e_G using $k = 0.95$ is greater than using $k = 0.99$ and smaller than using 0.9 in the initial two steps. However, it decreases faster than the other two cases in the latter steps. The number of new points in the case with $k = 0.95$ makes h-adaptivity more efficient than using the other two cases, achieving a better convergence with more accurate results. Figure 8(b) shows the convergence rates of $||e||_{L_2}$ in uniform refinement and h-adaptivity with $k = 0.9, 0.95, 0.99$, which is used to validate the performance of the proposed global error measure e_G. Comparing Figure 8(a) with Figure 8(b), recalling that this is a 1D problem with

an analytical solution, a similar trend is apparent using e_G and $||e||_{L_2}$ with different k, although the magnitudes in these two figures are different.

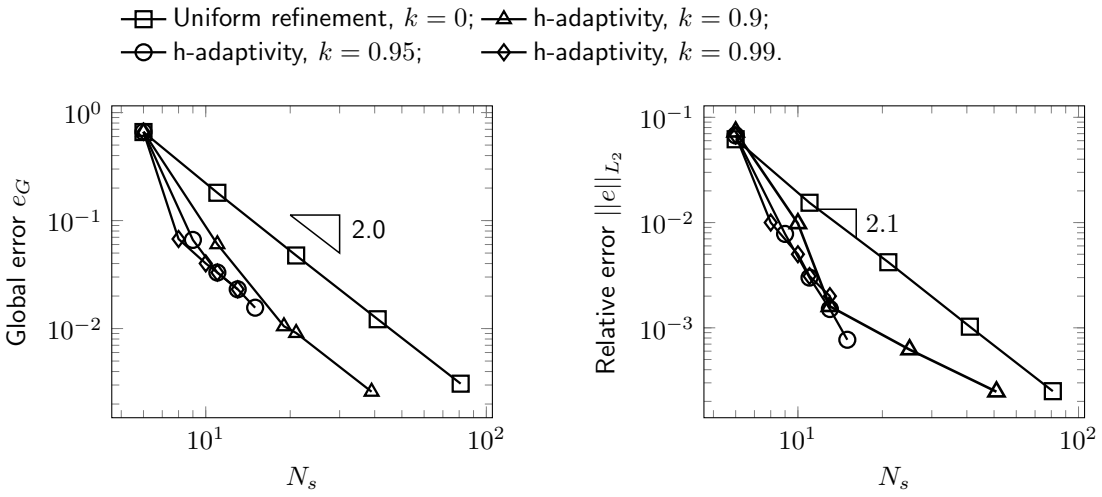

(a) Convergence rate of e_G; (b) Convergence rate of $||e||_{L_2}$.

Figure 8: Convergence rate of the 1D bar problem using uniform refinement and h-adaptivity with various k.

Measurements of e_G versus the CPU time (which includes the total computational time for calculation, error estimation and point refinement) and the effectivity index θ for h-adaptivity with different local refinement coefficients k, are shown in Figure 9. It can be seen in Figure 9(a) that uniform refinement takes more time than h-adaptivity to achieve the prescribed accuracy since in h-adaptivity fewer points are used than in uniform refinement. Comparing the CPU time in h-adaptivity with varying k, the computational cost using $k = 0.9$ is higher than using $k = 0.95$ and $k = 0.99$ as more new points are inserted. Fewer new points are inserted using $k = 0.99$, but it is slower to achieve the predefined accuracy. From the above numerical results, for this problem h-adaptivity with $k = 0.95$ can achieve better accuracy for less CPU time than uniform refinement or h-adaptivity with other k values. In Figure 9(b), the effectivity index with $k = 0.9, 0.95, 0.99$ in h-adaptivity for this 1D problem is plotted. The effectivity index for $k = 0.95$ increases slightly in the continuous adaptive steps and the gradient of θ is not a constant as the convergence rates of errors described by different error estimators have different magnitudes. The effectivity index with $k = 0.9$ shows oscillation around a value 10, which implies the ratio of the proposed error estimator and the actual error is close to a constant. The global error estimator e_G converges at a similar rate to the actual errors.

Distributions of collocation points and local errors, e_l and $||e||_{L_2}$ of each local length in the step-by-step h-adaptivity with $k = 0.95$, are shown in Figure 10. It can be observed that the local lengths with local errors e_l and $||e||_{L_2}$ greater than the permissible errors are refined in h-adaptive process. In this figure, e_l and $||e||_{L_2}$ follow the same trend although they are estimated in different ways. In Figure 10(b)-10(d), the positions of newly added collocation points can be determined by e_l or $||e||_{L_2}$. It can

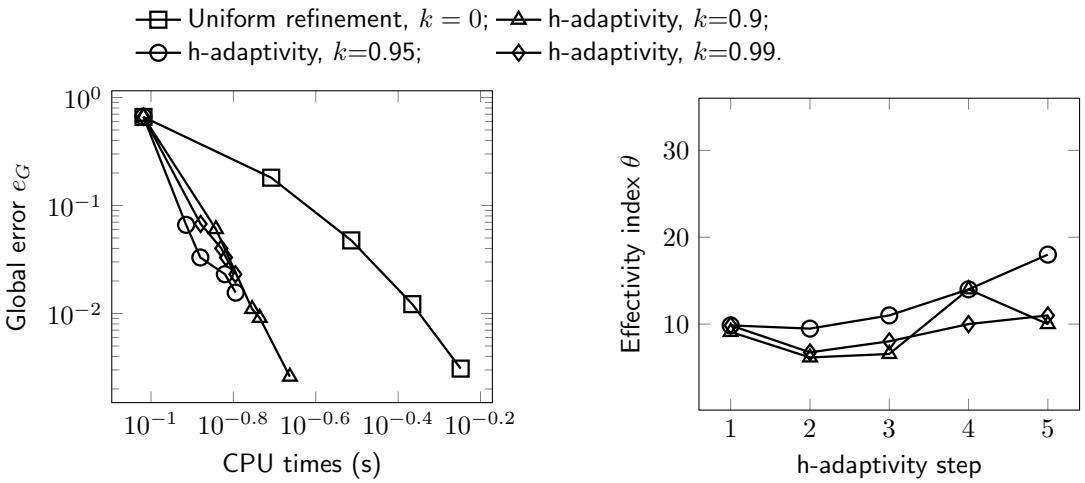

(a) Convergence rate of e_G against CPU time; (b) The effectivity index.

Figure 9: Computational efficiency and the effectivity index of the 1D bar problem using h-adaptivity using various k with $N_s^* = 2$.

also be observed in Figure 10 that there is only a little variation in the local errors across the domain, therefore the selections of refinement coefficient k are in a small range and sensitive to the analysis. Since all local errors are very close to the maximum local error estimator, k is chosen to be close to 1 (here $k = 0.9, 0.95$ and 0.99). If values of k are chosen in a larger range, some choices below a certain value may actually lead to analyses which have identical results with uniform refinement ($k = 0$). It is clear that the selection of the best local refinement parameter varies with problems and distribution of local errors.

6.2. An infinite plate with a circular hole

In this example, an infinite plate with a circular hole of radius a=1 with a far field stress $p = 1$ in the x-direction under a plane stress condition is analysed. In this example, uniform refinement, pure r-, h- and combined rh-adaptivities are compared in terms of accuracy and computational cost. Because the problem model is symmetric, the upper right quarter of the infinite plate, truncated at $x = 5$ and $y = 5$ ($b = 5$), is taken for analysis, as shown in Figure 11. Displacement boundary conditions were imposed at the collocation points on the the right and top edges, and roller boundary conditions were imposed on the bottom and left edges and the circular edge was traction free. The governing PDE was applied to the rest of the collocation points in the interior of the domain. This problem has been widely used for validation of numerical methods in the past and the analytical solution of displacement [85] is

$$u = \frac{a}{8G}\left\{\frac{r}{a}(\kappa+1)\cos\theta + \frac{2a}{r}[(1+\kappa)\cos\theta + \cos(3\theta)] - \frac{2a^3}{r^3}\cos(3\theta)\right\} \tag{31}$$

$$v = \frac{a}{8G}\left\{\frac{r}{a}(\kappa-3)\sin\theta + \frac{2a}{r}[(1-\kappa)\sin\theta + \sin(3\theta)] - \frac{2a^3}{r^3}\sin(3\theta)\right\}, \tag{32}$$

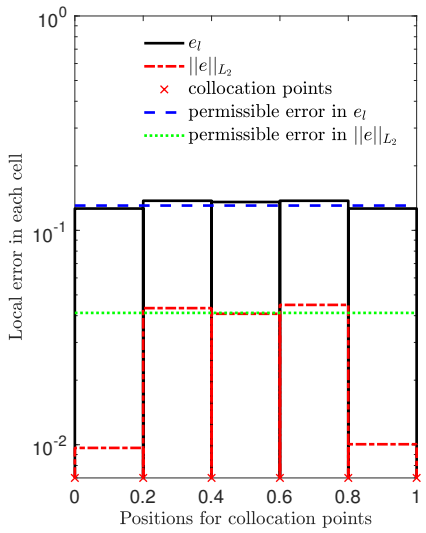

(a) The initial calculation;

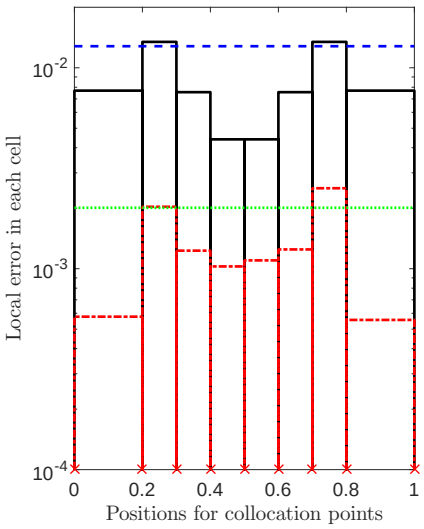

(b) The first h-adaptive step;

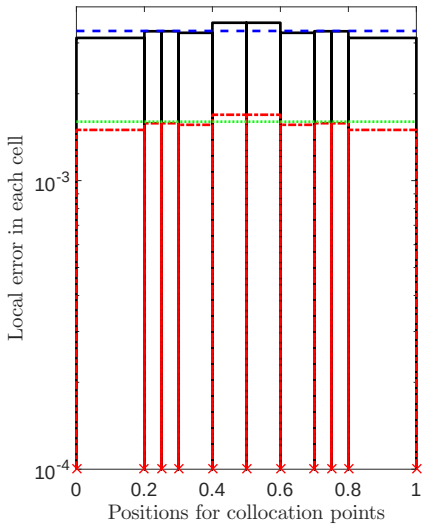

(c) The second h-adaptive step.

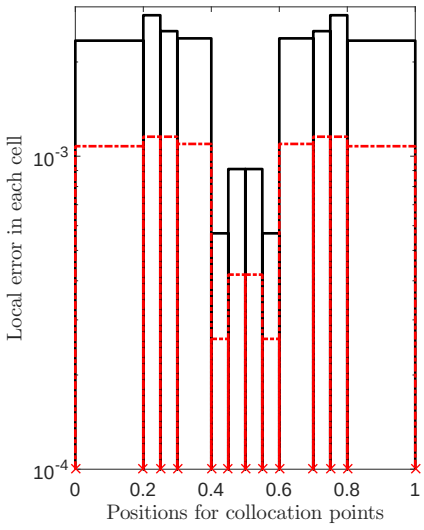

(d) The third h-adaptive step.

Figure 10: The collocation points and local error distributions in h-adaptivity with $k = 0.95$ of the 1D bar problem.

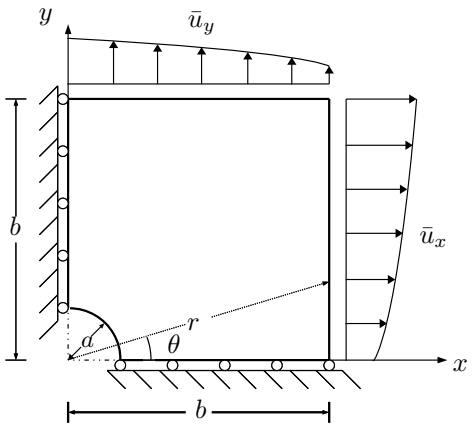

Figure 11: A portion of the infinite plate with a circular hole with a far field stress $p = 1.0$ in x direction.

where u and v are displacements in x and y directions, E is the modulus of elasticity, ν is Poisson's ratio, G is the shear modulus

$$G = \frac{E}{2(1+\nu)}, \tag{33}$$

and

$$\kappa = \frac{3-\nu}{1+\nu}. \tag{34}$$

r and θ are the polar coordinates as shown in Figure 11. The problem here was solved with $E = 10^6$ and $\nu = 0.3$. Throughout, a value of $N_s^* = 3$ was used. In the initial distribution, 63 collocation points were distributed in the interior of the problem domain and on the boundaries as shown in Figure 12(a). Collocation points on boundaries were fixed normal to the boundaries in r-adaptivity. The local error estimator e_t for each local area was estimated at the generated calculation points and $k = 0.2$ in this example was selected to test the performance of various adaptive strategies. Unlike in the 1D bar problem, the smaller local refinement coefficient k is used in this example since the variation of local errors is more significant as compared to the 1D problem.

The distributions of collocation points in the first rh-adaptivity step are illustrated in Figure 12. In r-adaptive step, collocation points in the initial distribution are moved towards the circular hole area as shown in Figure 12(b), where the blue arrows illustrate the moving direction and distance of each collocation point determined by the material equilibrium residuals. Error residuals around the circular hole are higher than in the other local areas because of the stress concentration effect caused by the circular hole. These updated positions of collocation points are employed to construct the Delaunay triangulation where three calculation points are generated in each triangulation as shown in Figure 12(c). In the following h-adaptivity step, as shown in Figure 12(d), most of the newly added points are again located in the area close to the hole.

Since the analytical solution exists, the L_2 norms of relative error in terms of the displacement $||e||_{L_2}$ for uniform h-refinement, pure h-, r- and combined rh-adaptivities are plotted in Figure 13. These

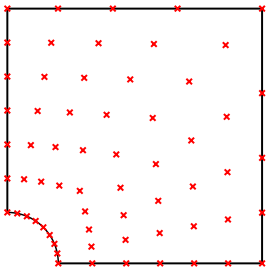

(a) A portion of the infinite plate with a circular hole with a far field stress $p = 1.0$ in x direction.

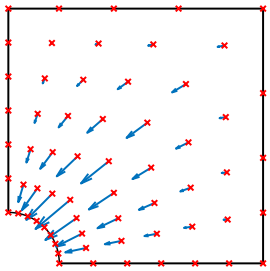

(b) Collocation points after the 1st relocation.

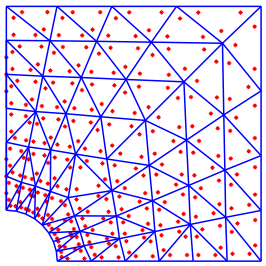

(c) The generation of triangles and calculation points.

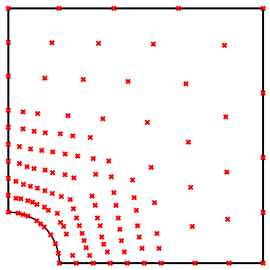

(d) Collocation points after the 1st rh-adaptivity.

Figure 12: The distribution of collocation points in rh-adaptivity with $k = 0.2$ of the infinite plate with a circular hole problem.

four strategies start with the same number of degrees of freedom. The convergence rate for uniform refinement is 2.0, which agrees well with the expected convergence rate for the MEPCM. Values of $||e||_{L_2}$ in h-adaptivity are smaller and have a higher convergence rate than for uniform refinement using the same discretisation. It can be seen that the convergence rate of $||e||_{L_2}$ for r-adaptivity is almost the same as for uniform refinement as they use the same basis functions; i.e. the improvement of accuracy between uniform and r-adaptivity for different discretisations stays approximately the same. The fourth set of plotted results is for the rh-adaptive process which is adopted five times from the same initial number of degrees of freedom as in the other cases. It is observed that $||e||_{L_2}$ in the combined rh-strategy exhibits a better convergence rate than uniform, r- and h-adaptivities. In rh-adaptivity, N_c and N_s increase from 63 to 1213 over five steps. After the initial calculation, the accuracy of the solution is improved by r-adaptivity where the number of degrees of freedom remains the same indicated by the vertical section of the plot in Figure 13. In the following h-adaptive step, the errors are reduced by increasing the number of degrees of freedom. Not only are the collocation points relocated in r-adaptivity but also additional points are refined in a combined strategy, which gives a more flexible approach with better performance in terms of accuracy than individual adaptive strategies. This elastic plate with a circular hole problem has also been studied in [37] and relative errors between exact and estimated results in the energy norm using uniform and h-adaptive IGA-C has been demonstrated. It was observed in [37] that the convergence rates in uniform and adaptive Gaussian collocation methods are 1.4 and 1.9, which is faster than using Greville and Galerkin collocation methods. Fig. 13 shows the convergence rate of $||e||_{L_2}$ using the h-adaptive MEPCM which is higher than 2.0. However, as indicated above, the error estimators are different, and together with the major differences in the basis functions and the discretizations probably invalidates a direct and reliable comparison without further study.

For h- and rh-adaptive approaches, the global error estimator e_G obtained in each h-adaptive step is shown in Figure 14, where it is clear that e_G converges faster in rh-adaptivity than in h-adaptivity. Comparing $||e||_{L_2}$ in Figure 13 with e_G in Figure 14, although the actual values of e_G and $||e||_{L_2}$ for this example are different, they show the same changing trend and the proposed e_G can be used to predict the distributions of actual errors.

Figure 15 shows the material force residuals in each r step of combined rh-adaptivity. It can been seen in Figure 15 the minimisation of material force residual becomes more efficient from the second r-adaptive step because h-adaptivity is used after the first r-adaptive step, which reduces the discretisation error.

The computational costs of using these strategies are presented (in Table 2). It is obvious that uniform refinement costs the shortest CPU time using the MEPCM with $N_s = 1225$. The pure h-adaptive approach starts from $N_s = 63$ to $N_s = 1213$ and the CPU time for h-adaptivity includes 5 calculations, 5 error measurements and 5 point refinements in total, taking 820.2s which is nearly

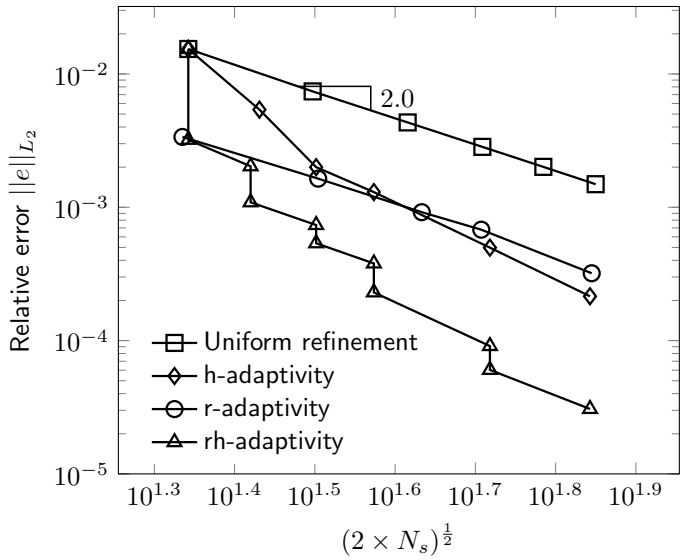

Figure 13: Convergence rate of $||e||_{L_2}$ of the plate with a circular hole problem with $k = 0.2$.

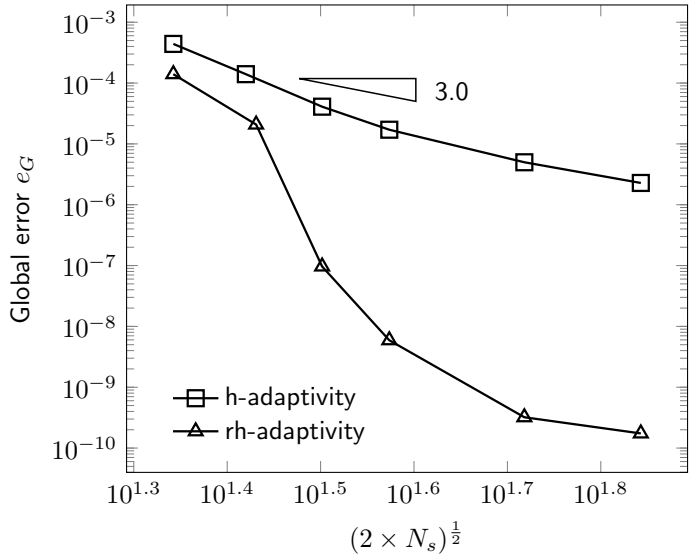

Figure 14: Convergence rate of e_G using h and hr-adaptivity of the plate with a circular hole problem with $k = 0.2$.

	Initial N_s	Final N_s	CPU time (s)	Final $\|\|e\|\|_{L_2}$	Final e_G
Uniform refinement	1225	1225	7.760×10^{1}	1.490×10^{-3}	1.66×10^{-05}
h-adaptivity	63	1213	8.202×10^{2}	2.101×10^{-4}	2.280×10^{-06}
r-adaptivity	1225	1225	1.232×10^{3}	3.199×10^{-4}	3.554×10^{-06}
rh-adaptivity	63	1213	1.923×10^{3}	9.072×10^{-5}	1.741×10^{-10}

Table 2: Quantitative results for the infinite plate with a circular hole problem using different adaptivity approaches.

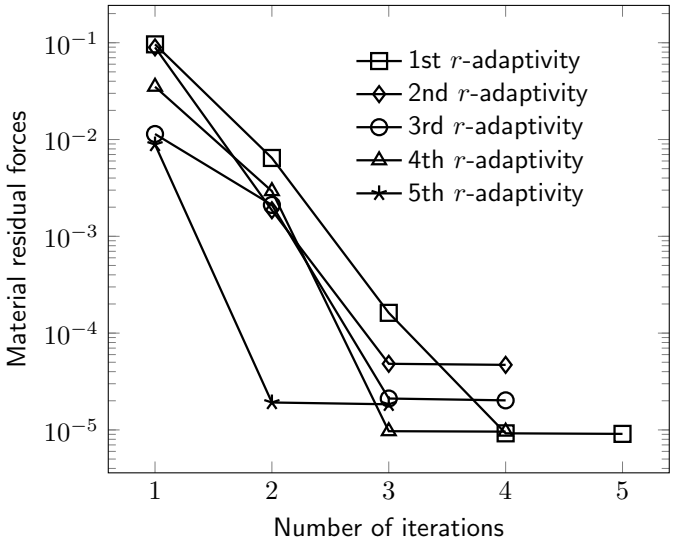

Figure 15: The material force residuals against iterations for the plate with a circular hole problem, with $k = 0.2$.

10 times that of uniform refinement. The pure r-adaptive approach relocates 1225 collocation points and the total CPU time for this process is 15.8 times greater than uniform refinement but the error is cut by 78.5%. The total CPU time for combined rh-adaptivity is also reported. Compared to pure h-adaptivity, the combined approach reduces 99.9% of the error but at greater cost. Clearly for practical analyses one would be seeking to maximise the ratio of accuracy to cost, so a high computational cost does not entirely rule out one approach over another.

6.3. L-shaped plate under uniaxial loading

The final example presented in this paper is that of a plane stress L-shaped plate subjected to uniform displacement on one external edge, for which the problem model and boundary conditions are shown in Figure 16. The right and top edges were constrained in x and y directions, respectively, and Dirichlet boundary conditions were imposed on the left edge. The other three edges were traction free. The material properties used for this example were $E = 1.0 \times 10^5$ and $\nu = 0.3$. An analytical solution is not available for this example so it is impossible to work out $||e||_{L_2}$. The proposed e_G in h-adaptivity is therefore adopted to identify the accuracy of the local approximation in the h- and rh-adaptive processes.

Again, uniform h-refinement, pure r-, h- and combined rh-adaptive approaches were considered for comparison in terms of accuracy and computational cost for this example. $N_s^* = 3$ was selected throughout and $k = 0.3$ used in h-adaptivity. The local errors vary considerably in this example because of the stress singularity at point C so the selection of k is smaller than that of the first example. Collocation points on boundaries were fixed in r-adaptivity. At the beginning of the analysis, 96 collocation points were distributed uniformly with the same number of source points but at slightly different positions, as shown in Figure 17(a). All source points were distributed non-uniformly in radial

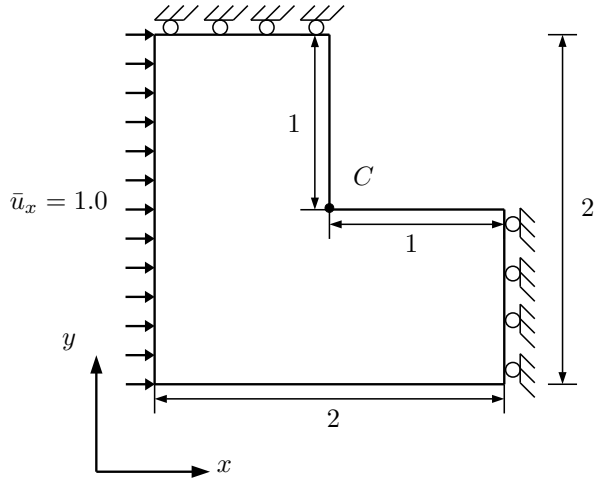

Figure 16: The L-shaped plate with a uniform displacement on the left edge.

direction centred at point C by a scaling parameter 0.01.

As shown in Figure 17(b) collocation points in the interior of the domain were relocated in the r-adaptive step, resulting in a distribution that concentrates a group of collocation points towards the stress singularity at C, while the collocation points on boundaries were not allowed to move. The moving direction and distance of each collocation point have been marked by the blue arrows. The updated collocation points in Figure 17(b) are employed to generate Delaunay triangulations, for which three calculation points are produced in each triangle as shown in Figure 17(c). Local errors are measured at calculation points, which determines the positions for new collocation points in h-adaptive step. In Figure 17(d) it is seen that new collocation points are inserted around point C. In both r- and h-adaptive processes, collocation points are inserted near to and moved towards the singularity point since the material force residual and e_t are much higher there than in the rest of the domain as might be expected.

The global error e_G is also calculated to assess the accuracy of uniform refinement, r-, h- and rh-adaptivities, as shown in Figure 18. The global error e_G in uniform refinement reduces more slowly with higher error values than the other three methods. h-adaptivity improves the accuracy more efficiently with a greater convergence rate than that of uniform refinement. For the same number of degrees of freedom, new collocation points are refined in the regions with higher e_t, such as near point C in this example. In uniform refinement, e_t in some regions far away point C reaches the prescribed accuracy requirement where additional collocation points are not needed. Although the material force residuals are used as an error estimator in the Newton-Raphson method in r-adaptivity, e_G is also calculated after each r-process as a consistent error estimator to compare the convergence rate with the other three strategies. r-adaptivity decreases e_G using the same number of degrees of freedom and shows a similar convergence rate to uniform h-refinement. Given the fact that errors have more than one

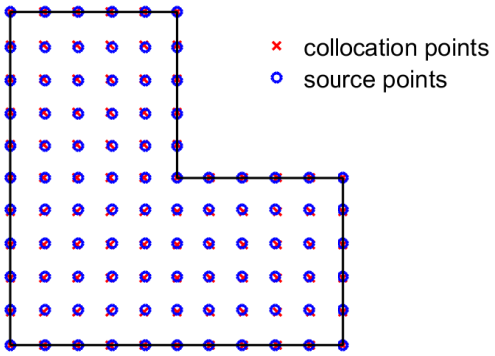

(a) Collocation and source points.

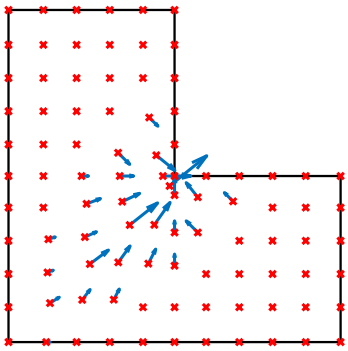

(b) Collocation points after the 1st relocation.

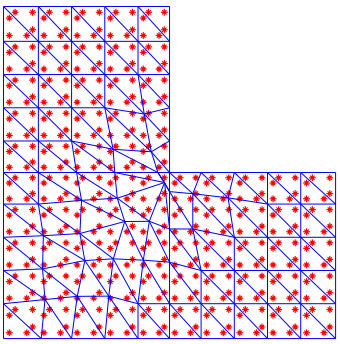

(c) The generation calculation points in triangles.

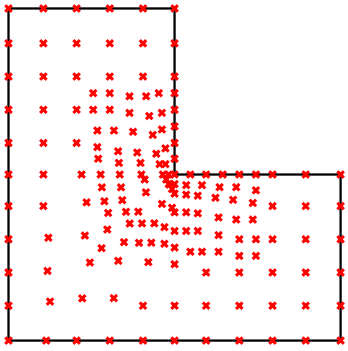

(d) Collocation points after the 1st refinement.

Figure 17: The generation of points and triangulations of rh-adaptivity of the L-shaped plate.

source, the r-adaptive procedure can only eliminate part of the discretisation errors by minimising the material force residual.

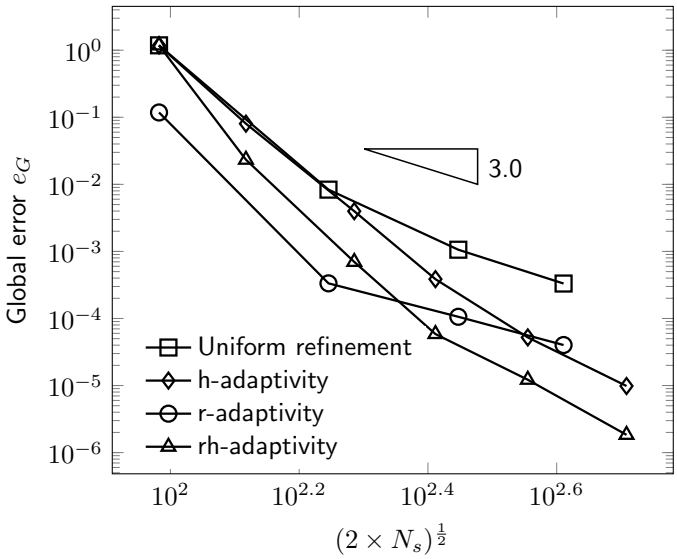

Figure 18: Convergence rate of e_G using different adaptivity of the L-shaped plate with $k = 0.3$.

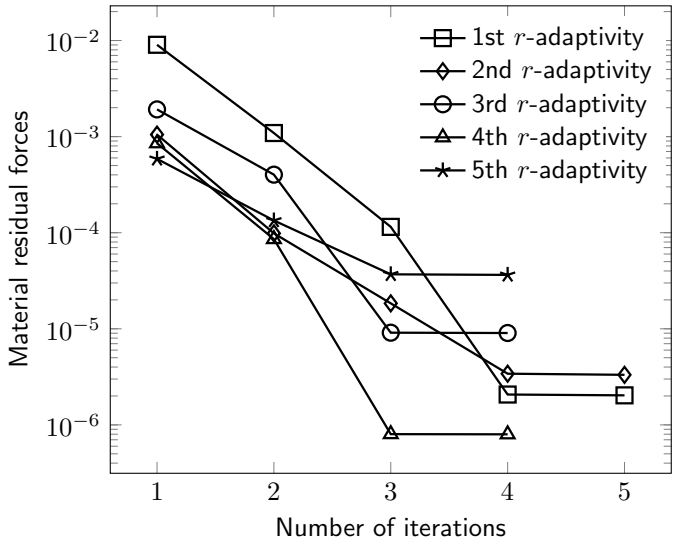

Figure 19: Material force residuals in the iteration process of the L-shaped plate with $k = 0.3$.

The material force residuals measured in the 5 r-adaptive steps of a combined rh-adaptivity are shown in Figure 19. In the 5 r-adaptivity steps, collocation points' relocations are completed within 5 iterations to achieve the prescribed requirement. The absolute value of residual in the first r-adaptivity step is higher than the rest because h-adaptivity is implemented after the first r-process.

For this example, Table 3 presents the CPU time for different adaptive strategies. The CPU time for h-adaptivity is counted when N_s is increased from 96 to 357 which includes 4 MEPCM calculations, 4

error estimations and 4 point refinements. Both source and collocation points are refined in each process and basis functions and derivatives are recalculated. This repeated process costs much more CPU time (3 times) than uniform h-refinement but with a significant accuracy improvement. In r-adaptivity, 408 collocation points are relocated iteratively and, compared to uniform refinement, an additional 184s is spent on relocation. The combined adaptive procedure is repeated 4 times which takes more time than the summation of pure h- and pure r-adaptivity since single h- and r-adaptive process are dependent on each other. The error estimation in each adaptivity step relies on the solution obtained from the previous step. However this combined method provides a more flexible way to achieve the best accuracy in contrast to the other three adaptivity processes.

	Initial N_s	Final N_s	CPU time (s)	Final e_G
Uniform h-refinement	408	408	9.119×10^1	3.325×10^{-4}
h-adaptivity	96	357	2.257×10^2	9.84×10^{-6}
r-adaptivity	408	408	2.752×10^2	4.024×10^{-5}
rh-adaptivity	96	511	5.224×10^2	1.845×10^{-6}

Table 3: Quantitative results for the L-shaped plate.

7. Conclusions

In this work, r-, h- and combined rh-adaptive strategies have been investigated and implemented with the MEPCM for the first time. The discrete material force residuals act as driving forces in r-adaptivity determined from the imbalance of material equilibrium equation for these linear elasticity problems. r-adaptivity results in an optimal distribution of collocation points with minimum total potential energy achieved by collocation point relocation using a certain number of degrees of freedom. h-adaptivity offers a point refinement strategy to achieve better accuracy that reduces errors by satisfying the physical equilibrium at more collocation points than at the original arrangement of points. Therefore, in this paper, a robust error estimate based on the strong form of the governing equations residual and a clear refinement procedures have been developed. The selection of refinement parameter k value, which has an effect on the efficiency of h-adaptivity in terms of accuracy and computational cost, is difficult. k appears to be dependent on the requirement of prescribed accuracy in adaptivity and the problem geometry with boundary conditions and external loads. Although there is no rigorous rule to define the value of k, this is a common issues across adaptive numerical analysis and its value can be suggested by the variation of local errors. A combined adaptive technique has also been developed in which r- and h-adaptivities are repeated in cycles to achieve a prescribed tolerance. Numerical examples are presented to demonstrate the proposed adaptive strategies. A comparison in terms of the convergence characteristics in L_2 norm of relative error and proposed relative error norm on material force residual for a problem with an analytical solution indicates that r-adaptivity is more flexible than

uniform h-refinement. Another comparison between h-adaptivity and uniform h-refinement verifies that the error estimator in h-adaptivity is stable. Both r- and h-adaptivities can achieve better accuracy with higher convergence rates than uniform refinement but at greater cost. 2D problems with and without analytical solutions were also examined using combined rh-adaptivity. In conclusion, clear evidence of satisfactory convergence has been provided throughout this paper depending on the different adaptive MEPCMs used. The computational cost of using combined rh-adaptivity is greater than single adaptive strategies and uniform refinement, however it is important to remember that a practical problem will be seeking a prescribed accuracy as well as seeking to reduce computational cost.

This work has introduced combined rh-adaptivity in the MEPCM for the first time and has been validated against 1D and 2D problems. It would be interesting to extend the proposed rh-adaptive MEPCM for solving 3D problems. However, more effort is required to construct 3D max-ent basis functions with second derivatives, as well as to assemble the coefficient matrix in 3D. Correspondingly, the complexities in adaptive strategies are also increased with more expensive computational cost. It could be an interesting topic of future research.

Acknowledgements

This work has been sponsored by the China Scholarship Council (CSC) and the Department of Engineering, Durham University.

Appendix A Derivation of material equilibrium

In Appendix A, the derivation of material equilibrium is presented, which is based on the material in [75]. The Cauchy stress for small deformations can be written as

$$\sigma_{ij} = \frac{\partial W}{\partial \varepsilon_{ij}}, \tag{35}$$

with strain

$$\varepsilon_{ij} = \frac{1}{2}(u_{i,j} + u_{j,i}), \tag{36}$$

where $i, j = 1, 2$ in 2D. Total potential energy stored in elastic body is defined as

$$W = W(u_i, u_{i,j}, x_i) \tag{37}$$

where W is a function of $u_i, u_{i,j}$ and x_i. Using the chain rule, the spatial gradient of strain energy with respect to each particle of the medium x_l is given by

$$\frac{\partial W}{\partial x_l} = \frac{\partial W}{\partial u_i} u_{i,l} + \frac{\partial W}{\partial u_{i,j}} u_{i,jl} + \frac{\partial W}{\partial x_l}\Big|_{\text{explicit}}, \tag{38}$$

where $\frac{\partial W}{\partial x_l}\Big|_{\text{explicit}}$ denotes the explicit derivative of strain energy with respect to x_l. In Eq. (38), using the relationship $\frac{\partial W}{\partial u_i} = f_i^b$ and $\frac{\partial \sigma_{ij}}{\partial x_j} = \frac{\partial}{\partial x_j}\frac{\partial W}{\partial u_{i,j}}$, we have $\frac{\partial W}{\partial u_i} = \frac{\partial}{\partial x_j}\frac{\partial W}{\partial u_{i,j}}$ considering physical

equilibrium. Then the first two terms on the right of Eq. (38) can be replaced by $\frac{\partial}{\partial x_j}\Big(\frac{\partial W}{\partial u_{i,j}}u_{i,l}\Big)$ using the chain rule inversely. Writing $\frac{\partial W}{\partial x_l} = \frac{\partial (W\delta_{ij})}{\partial x_l}$, the Eshelby stress or energy momentum tensor is defined as

$$\Sigma_{lj} = W\delta_{lj} - \sigma_{ij}u_{i,l}, \tag{39}$$

therefore Eq. (38) can be rearranged to obtain material equilibrium as

$$\frac{\partial \Sigma_{lj}}{\partial x_j} = \frac{\partial W}{\partial x_l}\Big|_{\text{explicit}}. \tag{40}$$

In r-adaptivity proposed in this work, the residual of material equilibrium is used as the source of the error estimator.

Appendix B Material equilibrium residual and its derivatives using the MEPCM in 1D case

For 1D problems, the strain energy in Eq. (16) is collected at collocation points using the MEPCM as

$$W \cong \sum_{c=1}^{N_c} \frac{E}{2}\{\frac{\partial u}{\partial x}\}_c^2 V_c. \tag{41}$$

The residual function and its derivative in Eq. (18) and Eq. (20) can be expressed as

$$R(x) = \frac{dW}{dx_c} = \sum_{c=1}^{N_c} E\{\frac{\partial u}{\partial x}\}_c\{\frac{\partial^2 u}{\partial x^2}\}_c V_c, \tag{42}$$

and

$$R'(x) = \sum_{c=1}^{N_c} E\Big(\{\frac{\partial^2 u}{\partial x^2}\}_c^2 + \{\frac{\partial u}{\partial x}\}_c\{\frac{\partial^3 u}{\partial x^3}\}_c\Big)V_c. \tag{43}$$

Using the MEPCM, $\frac{\partial u}{\partial x}$, $\frac{\partial^2 u}{\partial x^2}$ and $\frac{\partial^3 u}{\partial x^3}$ are the products of the first, second and third derivatives of local max-ent basis functions and displacement at source points.

References

[1] T. Belytschko, Y. Y. Lu, L. Gu, Element-free Galerkin methods, International Journal for Numerical Methods in Engineering 37 (2) (1994) 229–256.

[2] X. Zhang, X. H. Liu, K. Z. Song, M. W. Lu, Least-squares collocation meshless method, International Journal for Numerical Methods in Engineering 51 (9) (2001) 1089–1100.

[3] N. Aluru, A point collocation method based on reproducing kernel approximations, International Journal for Numerical Methods in Engineering 47 (6) (2000) 1083–1121.

[4] E. J. Kansa, Multiquadrics–A scattered data approximation scheme with applications to computational fluid-dynamics–I surface approximations and partial derivative estimates, Computers & Mathematics with Applications 19 (8-9) (1990) 127–145.

[5] E. J. Kansa, Multiquadrics–A scattered data approximation scheme with applications to computational fluid-dynamics–II solutions to parabolic, hyperbolic and elliptic partial differential equations, Computers & Mathematics with Applications 19 (8) (1990) 147–161.

[6] K. F. Kolsti, D. L. Kunz, A point collocation method for geometrically nonlinear membranes, International Journal of Solids and Structures 50 (2) (2013) 288–296.

[7] J. Zhang, G. Liu, K. Lam, H. Li, G. Xu, A gradient smoothing method (gsm) based on strong form governing equation for adaptive analysis of solid mechanics problems, Finite Elements in Analysis and Design 44 (15) (2008) 889–909.

[8] S.-W. Chi, J.-S. Chen, H.-Y. Hu, J. P. Yang, A gradient reproducing kernel collocation method for boundary value problems, International Journal for Numerical Methods in Engineering 93 (13) (2013) 1381–1402.

[9] W. Jiang, Z. Chen, A collocation method based on reproducing kernel for a modified anomalous subdiffusion equation, Numerical Methods for Partial Differential Equations 30 (1) (2014) 289–300.

[10] W. Chen, Z.-J. Fu, C.-S. Chen, Recent advances in radial basis function collocation methods, Springer, 2014.

[11] H. Hu, J. Chen, W. Hu, Weighted radial basis collocation method for boundary value problems, International Journal for Numerical Methods in Engineering 69 (13) (2007) 2736–2757.

[12] M. A. Jankowska, A. Karageorghis, C. Chen, Improved Kansa RBF method for the solution of nonlinear boundary value problems, Engineering Analysis with Boundary Elements 87 (2018) 173–183.

[13] M. Naisipour, M. H. Afshar, B. Hassani, A. R. Firoozjaee, Collocation discrete least square (CDLS) method for elasticity problems, International Journal of Civil Engineering 7.

[14] W. Khan, B. Ullah, et al., Analysis of meshless weak and strong formulations for boundary value problems, Engineering Analysis with Boundary Elements 80 (2017) 1–17.

[15] S. Fernandezmendez, A. Huerta, Imposing essential boundary conditions in mesh-free methods, Computer Methods in Applied Mechanics & Engineering 193 (12) (2004) 1257–1275.

[16] T. Belytschko, D. Organ, Y. Krongauz, A coupled finite element-element-free Galerkin method, Computational Mechanics 17 (3) (1995) 186–195.

[17] M. Arroyo, M. Ortiz, Local maximum-entropy approximation schemes: a seamless bridge between finite elements and meshfree methods, International Journal for Numerical Methods in Engineering 65 (13) (2006) 2167–2202.

[18] C. E. Shannon, A mathematical theory of communication, Bell System Technical Journal 27 (3) (1948) 379–423.

[19] E. T. Jaynes, Information theory and statistical mechanics, Physical Review 106 (4) (1957) 620.

[20] Z. Ullah, W. Coombs, C. Augarde, An adaptive finite element/meshless coupled method based on local maximum entropy shape functions for linear and nonlinear problems, Computer Methods in Applied Mechanics and Engineering 267 (2013) 111–132.

[21] D. Millán, A. Rosolen, M. Arroyo, Thin shell analysis from scattered points with maximum-entropy approximants, International Journal for Numerical Methods in Engineering 85 (6) (2011) 723–751.

[22] F. Amiri, D. Millán, Y. Shen, T. Rabczuk, M. Arroyo, Phase-field modeling of fracture in linear thin shells, Theoretical and Applied Fracture Mechanics 69 (2014) 102–109.

[23] F. Amiri, C. Anitescu, M. Arroyo, S. P. A. Bordas, T. Rabczuk, Xlme interpolants, a seamless bridge between xfem and enriched meshless methods, Computational Mechanics 53 (1) (2014) 45–57.

[24] C. J. Cyron, M. Arroyo, M. Ortiz, Smooth, second order, non-negative meshfree approximants selected by maximum entropy, International Journal for Numerical Methods in Engineering 79 (13) (2009) 1605–1632.

[25] A. Rosolen, D. Millán, M. Arroyo, Second-order convex maximum entropy approximants with applications to high-order PDE, International Journal for Numerical Methods in Engineering 94 (2) (2013) 150–182.

[26] A. Ortiz, M. Puso, N. Sukumar, Maximum-entropy meshfree method for incompressible media problems, Finite Elements in Analysis and Design 47 (6) (2011) 572–585.

[27] L. Fan, W. Coombs, C. Augarde, The point collocation method with a local maximum entropy approach, Computers & Structures 201(C) (2018) 1–14.

[28] F. Greco, M. Arroyo, High-order maximum-entropy collocation methods, Computer Methods in Applied Mechanics and Engineering 367 (2020) 113115.

[29] T. Belytschko, Y. Krongauz, D. Organ, M. Fleming, P. Krysl, Meshless methods: an overview and recent developments, Computer methods in applied mechanics and engineering 139 (1-4) (1996) 3–47.

[30] V. P. Nguyen, T. Rabczuk, S. Bordas, M. Duflot, Meshless methods: a review and computer implementation aspects, Mathematics and computers in simulation 79 (3) (2008) 763–813.

[31] O. C. Zienkiewicz, J. Z. Zhu, A simple error estimator and adaptive procedure for practical engineerng analysis, International Journal for Numerical Methods in Engineering 24 (2) (1987) 337–357.

[32] A. R. Diaz, N. Kikuchi, J. E. Taylor, A method of grid optimization for finite element methods, Computer Methods in Applied Mechanics and Engineering 41 (1) (1983) 29–45.

[33] F. Barros, S. Proença, C. de Barcellos, On error estimator and p-adaptivity in the generalized finite element method, International Journal for Numerical Methods in Engineering 60 (14) (2004) 2373–2398.

[34] J. Zhu, O. Zienkiewicz, Superconvergence recovery technique and a posteriori error estimators, International Journal for Numerical Methods in Engineering 30 (7) (1990) 1321–1339.

[35] O. Zienkiewicz, J. Zhu, Adaptivity and mesh generation, International Journal for Numerical Methods in Engineering 32 (4) (1991) 783–810.

[36] M. Kumar, T. Kvamsdal, K. A. Johannessen, Superconvergent patch recovery and a posteriori error estimation technique in adaptive isogeometric analysis, Computer Methods in Applied Mechanics and Engineering 316 (2017) 1086–1156.

[37] Y. Jia, C. Anitescu, Y. J. Zhang, T. Rabczuk, An adaptive isogeometric analysis collocation method with a recovery-based error estimator, Computer Methods in Applied Mechanics and Engineering 345 (2019) 52–74.

[38] I. Babuška, The selfadaptive approach in the finite element method, Mathematics of Finite Elements and Applications, Academic Press, London (1975) 125–142.

[39] O. C. Zienkiewicz, J. Z. Zhu, The superconvergent patch recovery and a posteriori error estimates. Part 1: The recovery technique, International Journal for Numerical Methods in Engineering 33 (7) (1992) 1331–1364.

[40] M. H. Afshar, A. R. Firoozjaee, Adaptive simulation of two dimensional hyperbolic problems by collocated discrete least squares meshless method, Computers & Fluids 39 (10) (2010) 2030–2039.

[41] M. Afshar, M. Naisipour, J. Amani, Node moving adaptive refinement strategy for planar elasticity problems using discrete least squares meshless method, Finite Elements in Analysis and Design 47 (12) (2011) 1315–1325.

[42] H.-J. Chung, T. Belytschko, An error estimate in the EFG method, Computational Mechanics 21 (2) (1998) 91–100.

[43] T. Belytschko, W. K. Liu, M. Singer, On adaptivity and error criteria for meshfree methods, Studies in Applied Mechanics 47 (1998) 217–230.

[44] H. Lu, J. Chen, Adaptive meshfree particle method, Lecture Notes in Computational Science and Engineering 26 (2002) 251–267.

[45] C. K. Lee, C. Zhou, On error estimation and adaptive refinement for element free Galerkin method: Part I: stress recovery and a posteriori error estimation, Computers & Structures 82 (4) (2004) 413–428.

[46] B. B. Kee, G. Liu, C. Lu, A least-square radial point collocation method for adaptive analysis in linear elasticity, Engineering Analysis with Boundary Elements 32 (6) (2008) 440–460.

[47] Q. Tang, K. Wei, G. Zhang, X. Sun, A fully automatic h-adaptive analysis procedure using the edge-based smoothed point interpolation method, International Journal of Computational Methods (2018) 1845001.

[48] J.-S. Chen, M. Hillman, S.-W. Chi, Meshfree methods: progress made after 20 years, Journal of Engineering Mechanics 143 (4) (2017) 04017001.

[49] G. R. Liu, B. B. T. Kee, L. Chun, A stabilized least-squares radial point collocation method (LS-RPCM) for adaptive analysis, Computer Methods in Applied Mechanics and Engineering 195 (37-40) (2006) 4843–4861.

[50] K. C. Cheung, L. Ling, Convergence Studies For An Adaptive Meshless Least-squares Collocation Method, International Journal of Computational Methods and Experimental Measurements 5 (3) (2017) 377–386.

[51] J. D. Eshelby, The force on an elastic singularity, Philosophical Transactions of the Royal Society 244 (877) (1951) 87–112.

[52] J. Eshelby, Energy relations and the energy-momentum tensor in continuum mechanics, in: Fundamental contributions to the continuum theory of evolving phase interfaces in solids, Springer, 1999, pp. 82–119.

[53] N. Kikuchi, Adaptive grid-design methods for finite element analysis, Computer Methods in Applied Mechanics and Engineering 55 (1-2) (1986) 129–160.

[54] R. Radovitzky, M. Ortiz, Error estimation and adaptive meshing in strongly nonlinear dynamic problems, Computer Methods in Applied Mechanics and Engineering 172 (1-4) (1999) 203–240.

[55] M. Braun, Configurational forces induced by finite-element discretization, Proceeding of Estonian Academy of Science. Physics. Mathematics 46 (1/2) (1997) 24–31.

[56] R. Mueller, G. Maugin, On material forces and finite element discretizations, Computational Mechanics 29 (1) (2002) 52–60.

[57] E. Kuhl, H. Askes, P. Steinmann, An ALE formulation based on spatial and material settings of continuum mechanics. Part 1: Generic hyperelastic formulation, Computer Methods in Applied Mechanics and Engineering 193 (39) (2004) 4207–4222.

[58] D. S. McRae, r-Refinement grid adaptation algorithms and issues, Computer Methods in Applied Mechanics and Engineering 189 (4) (2000) 1161–1182.

[59] P. Béal, J. Koko, R. Touzani, Mesh r-adaptation for unilateral contact problems, International Journal of Applied Mathematics and Computer Science 12 (2001) No–1.

[60] D. Materna, F.-J. Barthold, Configurational variations for the primal and dual problem in elasticity, ZAMM-Journal of Applied Mathematics and Mechanics/Zeitschrift für Angewandte Mathematik und Mechanik 89 (8) (2009) 666–676.

[61] R. Mueller, D. Gross, G. Maugin, Use of material forces in adaptive finite element methods, Computational Mechanics 33 (6) (2004) 421–434.

[62] A. Rajagopal, S. Sivakumar, Optimality of finite element grids based on material forces and error assessment, Computer Assisted Methods in Engineering and Science 12 (2006) 1–21.

[63] P. Thoutireddy, M. Ortiz, A variational r-adaption and shape-optimization method for finite-deformation elasticity, International Journal for Numerical Methods in Engineering 61 (1) (2004) 1–21.

[64] S. Riehl, P. Steinmann, On structural shape optimization using an embedding domain discretization technique, International Journal for Numerical Methods in Engineering 109 (9) (2017) 1315–1343.

[65] H. Askes, E. Kuhl, P. Steinmann, An ALE formulation based on spatial and material settings of continuum mechanics. Part 2: Classification and applications, Computer Methods in Applied Mechanics and Engineering 193 (39) (2004) 4223–4245.

[66] C. Pain, A. Umpleby, C. De Oliveira, A. Goddard, Tetrahedral mesh optimisation and adaptivity for steady-state and transient finite element calculations, Computer Methods in Applied Mechanics and Engineering 190 (29-30) (2001) 3771–3796.

[67] R. Mueller, S. Kolling, D. Gross, On configurational forces in the context of the finite element method, International Journal for Numerical Methods in Engineering 53 (7) (2002) 1557–1574.

[68] H. Askes, A. Rodríguez-Ferran, A combined rh-adaptive scheme based on domain subdivision. Formulation and linear examples, International Journal for Numerical Methods in Engineering 51 (3) (2001) 253–273.

[69] D. Materna, F.-J. Barthold, Goal-oriented r-adaptivity based on variational arguments in the physical and material spaces, Computer Methods in Applied Mechanics and Engineering 198 (41) (2009) 3335–3351.

[70] U. Basappa, A. Rajagopal, J. Reddy, Adaptive isogeometric analysis based on a combined r-h strategy, International Journal for Computational Methods in Engineering Science and Mechanics 17 (2) (2016) 73–92.

[71] A. Rajagopal, S. Sivakumar, A combined rh adaptive strategy based on material forces and error assessment for plane problems and bimaterial interfaces, Computational Mechanics 41 (1) (2007) 49–72.

[72] S. Riehl, P. Steinmann, An integrated approach to shape optimization and mesh adaptivity based on material residual forces, Computer Methods in Applied Mechanics and Engineering 278 (2014) 640–663.

[73] C. Peco, D. Millán, A. Rosolen, M. Arroyo, Efficient implementation of galerkin meshfree methods for large-scale problems with an emphasis on maximum entropy approximants, Computers & Structures 150 (2015) 52–62.

[74] O. Kardani, M. Nazem, M. Kardani, S. Sloan, On the application of the maximum entropy meshfree method for elastoplastic geotechnical analysis, Computers and Geotechnics 84 (2017) 68–77.

[75] J. Eshelby, The elastic energy-momentum tensor, Journal of Elasticity 5 (3-4) (1975) 321–335.

[76] E. Kuhl, P. Steinmann, Material forces in open system mechanics, Computer Methods in Applied Mechanics and Engineering 193 (23-26) (2004) 2357–2381.

[77] R. Gangadharan, A. Rajagopal, S. Sivakumar, An rh adaptive strategy based on material forces and error assessment, CMC-Tech Science Press 1 (2004) 229–244.

[78] T. Rabczuk, T. Belytschko, Adaptivity for structured meshfree particle methods in 2D and 3D, International Journal for Numerical Methods in Engineering 63 (11) (2005) 1559–1582.

[79] Z. Ullah, C. Augarde, Finite deformation elasto-plastic modelling using an adaptive meshless method, Computers & Structures 118 (2013) 39–52.

[80] Z. Ullah, C. E. Augarde, R. S. Crouch, W. M. Coombs, FE-EFGM coupling using maximum entropy shape functions and its application to small and finite deformation, in: 19th UK Conference of the Association for Computational Mechanics in Engineering (ACME), Heriot-Watt University, Edinburgh, 5-6 April, 2011, pp. 277–280.

[81] X. Zhuang, C. Heaney, C. Augarde, On error control in the element-free Galerkin method, Engineering Analysis with Boundary Elements 36 (3) (2012) 351–360.

[82] F. Greco, N. Sukumar, Derivatives of maximum-entropy basis functions on the boundary: Theory and computations, International Journal for Numerical Methods in Engineering 94 (12) (2013) 1123–1149.

[83] C. T. Kelley, Solving nonlinear equations with Newton's method, Vol. 1, Siam, 2003.

[84] T.-P. Fries, H. G. Matthies, Classification and overview of meshfree methods, Department of Mathematics and Computer Science, Technical University of Braunschweig.

[85] X. Zhuang, Meshless methods: theory and application in 3D fracture modelling with level sets, Ph.D. thesis, Durham University (2010).